Experimental Investigation of Micro Horizontal Axis Wind Turbine for Validation and Performance of an Optimized Blade by BEMT and CFD

By

Ahmad Zubair Hashim

Reg. No. 00000274610

Session 2018-20

Supervised by

Dr. Adeel Javed

US-Pakistan Center for Advanced Studies in Energy (USPCAS-E)

National University of Sciences and Technology (NUST)

H-12, Islamabad 44000, Pakistan

October 2021

Experimental Investigation of Micro Horizontal Axis Wind Turbine for Validation and Performance of an Optimized Blade by BEMT and CFD

By

Ahmad Zubair Hashim

Reg. No. 00000274610

Session 2018-20

Supervised by

Dr. Adeel Javed

A Thesis Submitted to the US-Pakistan Center for Advanced Studies in Energy in partial fulfillment of the requirements for the degree of MASTER of SCIENCE in

Energy Systems Engineering

US-Pakistan Center for Advanced Studies in Energy (USPCAS-E)

National University of Sciences and Technology (NUST)

H-12, Islamabad 44000, Pakistan

October 2021

THESIS ACCEPTANCE CERTIFICATE

Certified that final copy of MS/MPhil thesis written by **Mr. Ahmad Zubair Hashim** (Registration No. 00000274610), of US-Pakistan Center for Advanced Studies in Energy (USPCAS-E) has been vetted by undersigned, found complete in all respects as per NUST Statues/Regulations, is within the similarity indices limit and is accepted as partial fulfillment for the award of MS degree. It is further certified that necessary amendments as pointed out by GEC members of the scholar have also been incorporated in the said thesis.

Signature: _____

Name of Supervisor: _____

Date: _____

Signature (HoD): _____

Date:

Signature (Dean/Principal): _____

Date: _____

Certificate

This is to certify that work in this thesis has been carried out by **Mr. Ahmad Zubair Hashim** and completed under my supervision in Synthesis and Energy Storage laboratory, US-Pakistan Center for Advanced Studies in Energy (USPCAS-E), National University of Sciences and Technology, H-12, Islamabad, Pakistan.

Supervisor: _____

Dr. Adeel Javed
USPCAS-E
NUST, Islamabad

GEC member 1: _____

Dr. Majid Ali
USPCAS-E
NUST, Islamabad

GEC member 2: _____

Dr. Sehar Shakir
USPCAS-E
NUST, Islamabad

GEC member 3: _____

Dr. Hassan Abdullah Khalid
USPCAS-E
NUST, Islamabad

HOD-ESE: _____

Dr. Rabia Liaquat
USPCAS-E
NUST, Islamabad

Dean/Principal: _____

Dr. Adeel Waqas
USPCAS-E
NUST, Islamabad

Dedication

To my parents, who supported me in every aspect of life, and my siblings.

Abstract

Optimizing a blade for a small wind turbine to achieve a quick starting time at the loss of minimal power output is one of the most challenging aspects of design. This study considers a micro-wind turbine for experimental analysis to validate an optimized blade design based on blade element momentum theory and its performance analysis conducted numerically. The focus of the experiment was to improve the starting time considering different weight factors. 30 % power coefficient and 70 % starting time were considered during design. A scaled-down rotor of three blades optimized for both quick starting time and optimum power was manufactured by 3D printing. Polylactic Acid (PLA) was selected as a printing material to keep inertia equivalent to blades of the procured generator. The blades were mounted on a hub of a commercially available Wuxi 200 W wind turbine to carry out the experimental analysis in a controlled environment. Both wind speed and electric resistive loads were varied to achieve the desired tip speed ratio. It was observed that the rotational speed of the micro-wind turbine is affected by the resistive torque induced by the electric loads connected to the circuitry of the permanent electric generator. After the experiments, it was inferred that the optimized blade is well justified to operate in low wind conditions. The power outputs claimed by both blade element momentum theory and computational fluid dynamic analysis of the blade lag 40 % and 17 %, respectively. However, the experimental investigation shows superior starting time performance as it leads both the BEMT model and 6DOF analysis by 2.8 s and 3.25 s, respectively. The observed power coefficient at the tip speed ratio of 5.71 is 0.28 and that of the staring time is just 1 s. Cut in speed for the optimized blade was 3 m s^{-1} which is far better as claimed in blade element momentum theory i.e., 5 m $s^{-1,}$ and its performance analysis was conducted numerically. Therefore, this optimized blade design for micro-wind turbines is desirable for urban environments with wild wind resources.

Keywords: Tip Speed Ratio; Coefficient of Performance; Urban wind energy; horizontal axis wind turbine; starting performance optimization; computational fluid dynamics, experimental analysis.

Table of Contents

List of Figures

List of Tables

List of Publications

1. **Ahmad Zubair Hashim**, Adeel Javed, Saeed Iqbal, Syed Ali Abbas Kazmi "Experimental Investigation of an Urban-Scale Horizontal Axis Wind Turbine Rotor Optimized for Improved Starting Performance in Low Wind Speed Conditions"
   Journal: Sustainable Energy Technologies and Assessments, 2021 (**Submitted**)

List of Nomenclature

C_p	Power coefficient [-]
P	Power [W]
D	Rotor diameter [m]
R	Radius [m]
B	Number of blades
T	Time [s]
T_s	Starting time [s]
U	Wind speed [ms-1]
λ	Tip speed ratio [-]
ρ_d	Material density [kgm-3]
ρ_a	Air density [kgm-3]
η	Turbine efficiency [-]
P_a	Ambient Pressure [Pa]
P_1	Pressure Just Infront of Actuator Disk [Pa]
P_2	Pressure Just After of Actuator Disk [Pa]
U_u	Inlet Air Velocity [m s^{-1}]
U_d	Outlet Air Velocity [m s^{-1}]
U_t	Air Velocity at Turbine Disk [m s^{-1}]
A_u	Area of Turbine at Inlet [m^2]
A_t	Disk Area of Turbine [m^2]
A_d	Area of Turbine at Outlet [m^2]
TSR	Tip Speed Ratio
RPM	Rotation Per Minute
BEMT	Blade Element Moment Theory
CFD	Computational Fluid Dynamics
DAQ	Data Acquisition
CAD	Computer Aided Design
PLA	Poly Lactic Acid
ABS	Acrylonitrile Butadiene Styrene

PETG	Polyethylene terephthalate glycol
SWT	Small Wind Turbine
HAWT	Horizontal Axis Wind Turbine
VAWT	Vertical Axis Wind Turbine

Chapter 1 Introduction

1.1 Background

Fossil fuels are currently the dominant source of energy on a worldwide scale. In 2009, fossil fuels accounted for 89.2 percent of all commercially traded fuels [1]. Coal, natural gas, and oil are examples of fossil fuels. Because all of these resources occur naturally yet are non-renewable, new reserves must be located and utilised in order to sustain output. Oil is largely utilized for transportation, although coal and natural gas are commonly used to generate electricity. As the world gets increasingly industrialized, so will society's energy demands. Figures 1.1-1.3 show global fuel consumption for oil, natural gas, and coal since 1990. In all these figures, the dramatic expansion of world energy needs over the last quarter-century can be seen.

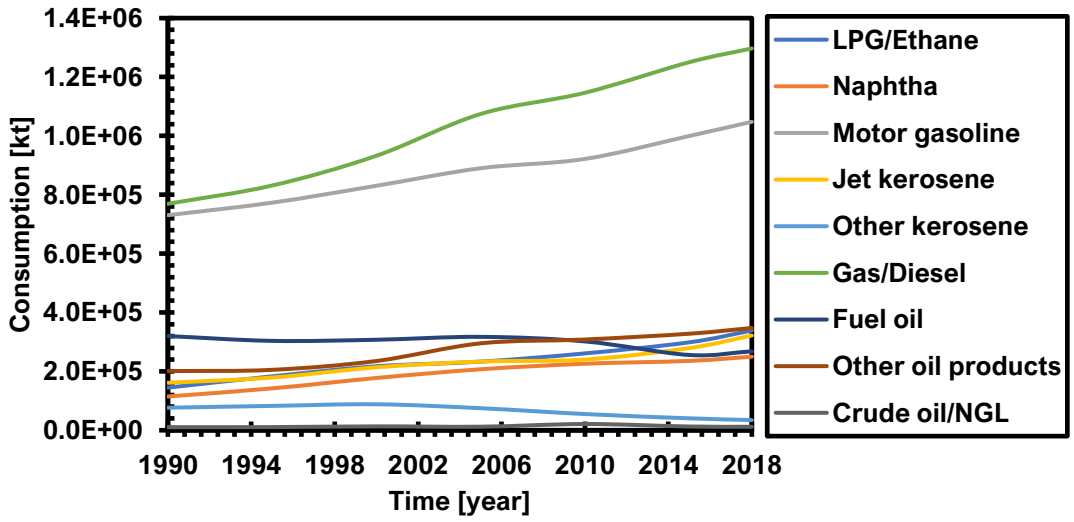

Figure 1.1 Word Oil Consumption [1]

As seen in Figure 1.1, diesel consumption has increased almost double since 1990. This increased drain on the available resources has led to further exploration for oil reserves in areas with greater extraction and transportation costs, such as offshore drilling. This in turn increases the cost of energy produced. Additionally, at some point, these reserves may become completely exhausted. The methodology when applied to world production predicts peak oil between 2009 and 2021 [2]. As seen in

Figure 1.1, this peak may have already occurred. At current consumption rates, the known oil reserves will be exhausted in 45.7 years [1].

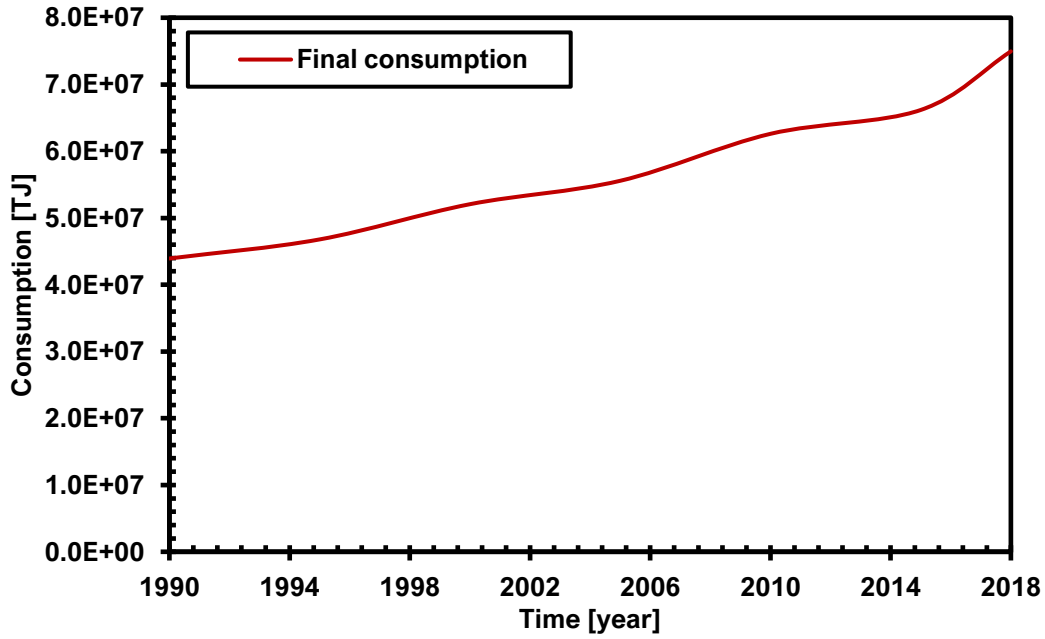

Figure 1.2 Worldwide natural gas consumption [1]

Natural gas consumption has increased by approximately 75% since 1990, shown in Figure 1.2. This increase can be attributed to the adoption of natural gas as a primary source for industrial power generation [3], due to the quick initialization time for natural gas plants. Although natural gas use declined for the first time in 2009 [1], the demand is predicted to continue to increase [3]. At the current rate of consumption, known natural gas resources will last 62.8 years [1].

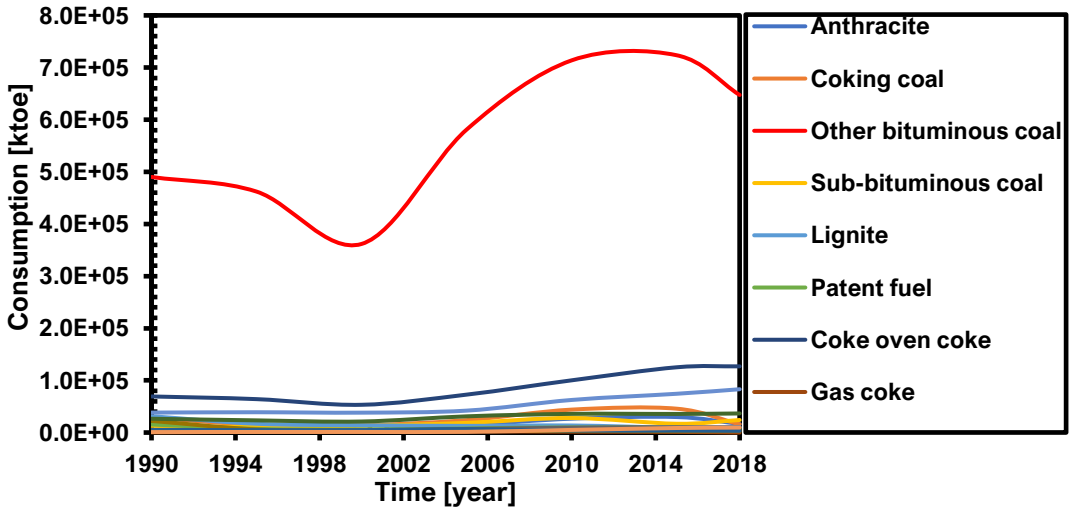

Figure 1.3 Worldwide coal consumption [1]

Figure 1.3 shows the coal consumption has greatly increased over the past 20 years that is driven by an increased energy demand in the developing world. The developing world prefers coal as an energy source due to its low economic cost. This lower cost is driven by the abundance of coal as a natural resource. At the current rate of consumption, known coal reserves will last 119 years [1]. However, coal has a much higher ecological cost than the other fossil fuels both in extraction and use. Natural gas has 70% fewer emissions during combustion than coal.

As shown above, the use of fossil fuel resources as the world's primary fuel source cannot continue indefinitely, even if world energy consumption is frozen. However, world energy usage is expected to rise by 44% from 2006 levels by the year 2030 [3]. The increasing demand for energy production combined with the depleted reserves of fossil fuels will create a much-increased cost for energy. This will create a strain on industrial growth and eventually could cripple the world economy, especially in developing countries that are driving their economic growth with energy generated by cheap fossil fuels.

Wind turbines were first employed for power generation in the early twentieth century; however, it wasn't until the 1970s oil crisis that windmills gained popularity as an alternative to oil-based energy. Today, the primary driver driving the development and implementation of wind power is global warming. [4].

Wind turbine technology is constantly advancing, necessitating more exact analysis. Since the movement of helicopter blades and windmill blades is so similar, this study was historically taken and modified from the analysis used for helicopter aerodynamics. Unstable blade-air loads and turbine functioning in linked and stalled flow may now be anticipated and understood as a result of these similarities. They've also improved the ability to predict tensile stresses and the aeroelastic response of rotating blades. The applicability of helicopter aerodynamics to wind turbine aerodynamics, on the other hand, is restricted. For example, wind turbines are subjected to a variety of atmospheric conditions that helicopters are not. In addition, wind turbines create abnormal environments. Examples include inconsistent wake impacts from tower shadows and influences from upstream towers.

Energy is a critical component of a country's socioeconomic development. Everything in this digital age is somehow intertwined with energy and electricity. The need for power in a country like Pakistan, where the population is growing at an exponential rate, is rapidly rising. Pakistan has endured the biggest energy crisis since its foundation in the previous decade, owing to a lack of long-term planning, inadequate management, and inefficient use of natural resources. Excessive use of fossil fuels produces drastic changes in climate change, and depletion of these resources also creates serious situations that need the search for alternative energy sources. Pakistan ranks second among the top ten countries most affected by climate change. Although Pakistan's contribution to global CO2 emissions is low when compared to developed countries, Pakistan is confronted with this issue due to its geological location. The value of renewable energy resources cannot be overstated in this situation. Currently, 60 percent of Pakistan's electricity output comes from thermal power plants, and their primary fuels are coal, natural gas, and liquefied natural gas (LNG), the majority of which are imported fuels that not only burden Pakistan's economy but also pose a possible threat to global warming. As a result, there is an urgent need to investigate alternative energy options to address this issue.

Renewable energy resources such as solar, wind, hydro, and biomass can be an ideal alternative to fossil fuels for power generation. Renewable energy has grown dramatically in the power sector during the last decade (2010-2019), from 414 GW to over 1650 GW, excluding hydropower. In 2018, renewable energy accounted for 12.9 percent of worldwide electricity generation [5]. Wind energy is the most potential renewable energy resource in terms of investment and renewable energy growth. According to a recent report published by the World Wind Energy Association, total wind energy installed capacity reached 597 GW in 2018 [6], with huge horizontal axis wind turbines accounting for the majority of the contribution. Small wind turbines are also in high demand, with the market reaching 945 MW in 2015 [6].

1.2 Global Wind Scenario and Scope of Wind Energy in Pakistan

On a local scale, wind behavior is difficult to anticipate. It is influenced by the local geography as well as the everyday weather conditions. However, substantial research into this behavior allows for broad geographical forecasts. The National Renewable Energy Laboratory has produced this data for wind turbine applications (NREL). The

wind potential of a location is classified by NREL into seven categories, which are presented in Table 1.1. Wind power density measurements at 10 m and 50 m elevations are shown in this table. The amount of energy available for extraction in a square meter of the area is referred to as wind power density. This table also includes the NREL ratings for each class in terms of potential generation. The Central United States is a major power generation region. Wind power has been used in many of these places as a collaborative effort with local farmers to increase earnings while preserving agricultural land. The energy generated in these places must then be transported to urban areas with high power demands. A rural region with low property prices near a city, manufacturing base, or high-capacity transmission line would be a good geographical site for wind power.

Table 1.1 Classes of wind power density at 10 m and 50 m

Wind Power Class	Resource Potential	10m		50m	
		Wind power density (W/m^2)	Speed(m/s)	Wind power density (W/m^2)	Speed(m/s)
1	Poor	0-100	0-4.4	0-200	0-5.4
2	Marginal	100-150	4.4-5.1	200-300	5.4-6.2
3	Moderate	150-200	5.1-5.6	300-400	6.2-6.9
4	Good	200-250	5.6-6.0	400-500	6.9-7.4
5	Excellent	250-300	6.0-6.4	500-600	7.4-7.8
6	Excellent	300-400	6.4-7.0	600-800	7.8-8.6
7	Excellent	>400	>7.0	>800	>8.6

Wind technology has rapidly risen in recent decades, with global wind power producing more than 50 GW in 2017 [7] as a result of lower equipment costs, favorable legislation, environmental concerns, and advancements in wind turbine technology. Wind energy is a type of renewable energy that is obtained indirectly. The worldwide economy is dependent on the availability of cheap and plentiful energy supplies, and wind energy provides an environmentally beneficial answer at a time when decreasing fossil fuel resources poses an existential danger to the environment and the global economy [8].

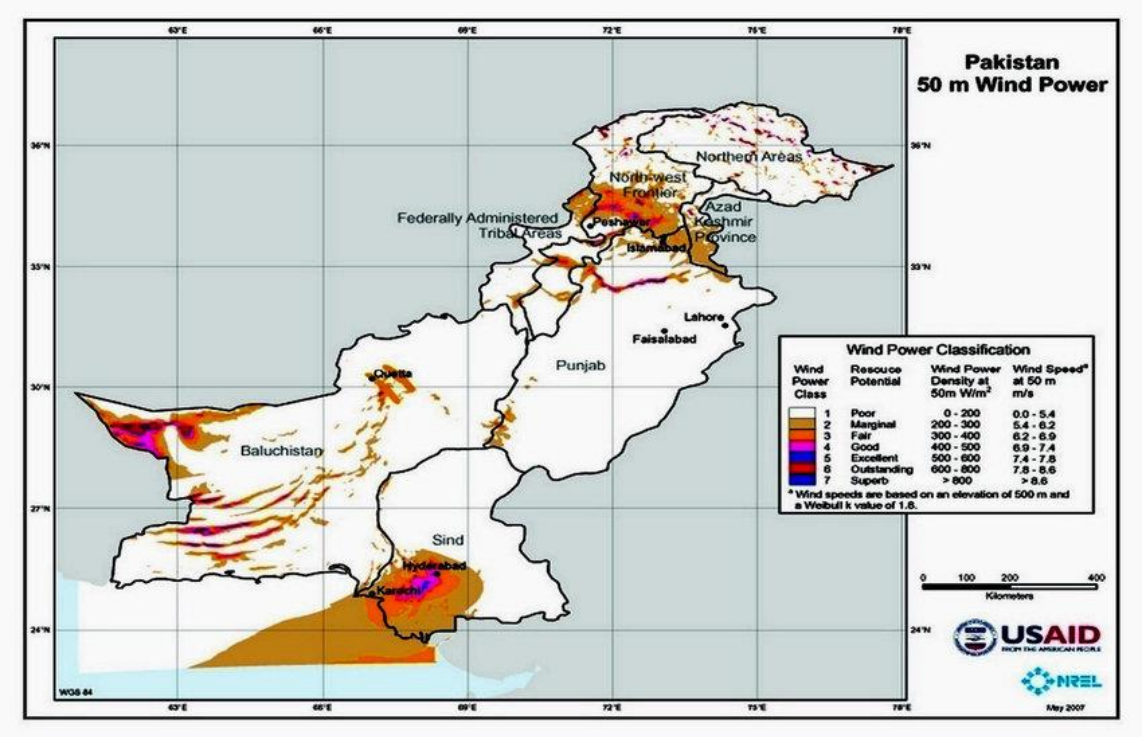

Figure 1.4 Wind Energy Map of Pakistan

Wind energy technology is quickly advancing, with the creation of giant rotor blades capable of extracting significant energy from the wind. Small wind turbines, a form of horizontal axis wind turbine, can play a significant role in distributing sustainable energy and providing solutions for off-grid places. A small wind turbine (SWT) has a swept area of fewer than 200 m^2, a rotor blade radius of 8 m or less, and a power output equal to or less than 50 kW. Furthermore, small wind turbines are classified into three classes based on their output power: micro 1 kW, mid 5 kW, and mini 50 kW [9].

1.3 Wind Turbines

Historically, power derived from sources such as coal, natural gas, and nuclear fuel was far less expensive than wind power. However, as the cost of fossil fuels rises and wind turbine technology improves, the playing field is leveling [10]. By 2016, the cost of electricity from a wind powered station will be equal to the energy from a natural gas electricity station in the windiest areas and coal fired electricity generation in very places [11]. Modern wind turbines have grown and capacity because of increased demand for wind turbine technology in recent years. Wind turbine rotor diameters can range from 5-100 m; however, they are frequently bigger than 50 m in diameter. Their

power generation capabilities vary widely as well, with some turbines producing only a few kilowatt-hours [10].

1.3.1 Wind Turbine Orientation

Wind turbines are classified into two types: horizontal axis wind turbines (HAWT) and vertical axis wind turbines (VAWT) (VAWT). Each orientation has advantages and downsides. VAWTs, also known as drag machines, use drag forces to rotate their blades. The primary benefit of a VAWT is that it functions regardless of the direction of the wind at any time of day or night. This means that no yaw system is required to line up the turbine in the course of the confrontation wind area. Blades are typically straight, with no taper along the long axis. This permits them to be produced at a lesser cost. Because they revolve about a vertical axis, the drive train can be situated close to the ground [10].

HAWTs, on the other hand, use lift forces in order to turn its blades and are commonly mentioned to as lift devices. HAWTs can be built with the turbine upstream or downstream of the supporting tower. The turbine inevitably lines up itself with the wind in the downstream version; this rotation is known as yaw. The rotor blades are somewhat tapered in the downwind direction to aid in their free yawing capacity. Tower wind shadow influences downstream HAWTs. A wake is created by the strengthening tower since it is located upstream of the rotor. The primary impact of this wake is irregular air packing on the blades, which results in an inconsistent angle of attack on the blades and stalling.

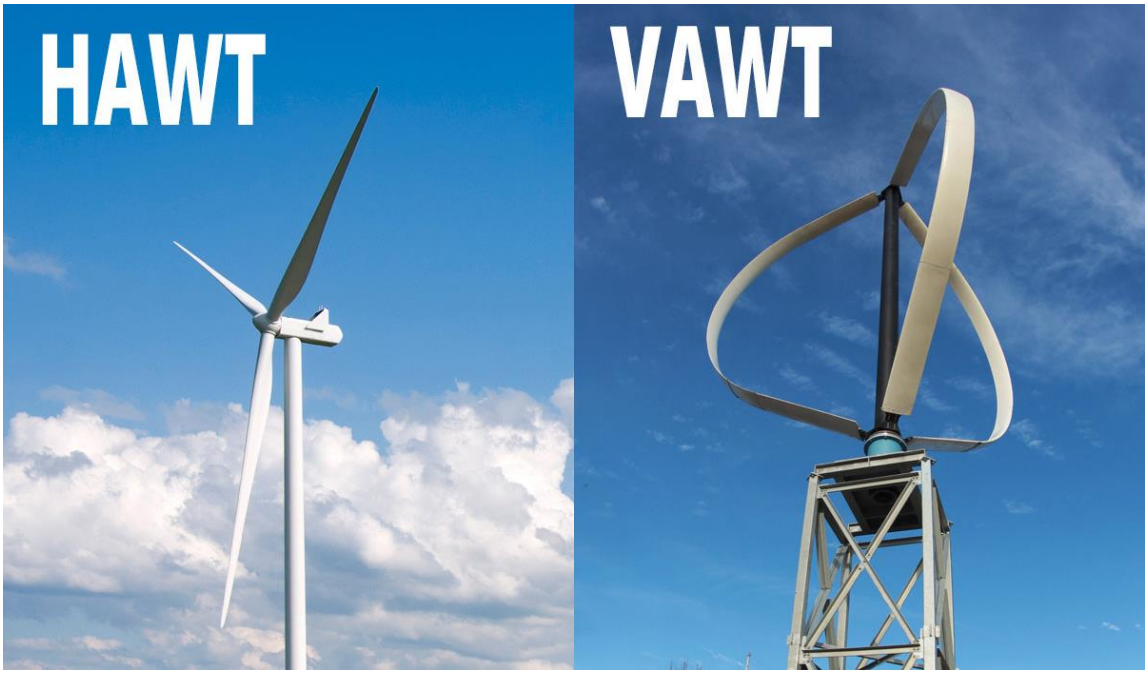

Figure 1.5 Horizontal axis wind turbine(left) and Verticle axis wind turbine(right)[12]

1.3.2 Induction Machine Construction

The rotor of an induction machine may be one of two types:

1.3.2.1 Squirrel cage

It has a rolling consisting of a succession of rods in the rotor holes that are short-circuited by end rings on both sides of the rotor. A vault rotor can be modelled as a symmetrical, short-circuited star-connected 3 phase wrapping with no availability to the rotor ‘windings' for analysis purpose.[13].

1.3.2.2 Wound rotor

A twisted rotor rotor has a 3-phase dispersed encircling with the equal quantity of batons as the stator coil. This rolling is typically associated in a star configuration, with the ends of the rolling carried out to three skid rings, allowing peripheral circuits to be attached to the rotor for monitoring motives [13].

There are usually two types of wind turbine rotors:

- Fixed speed rotors

- Variable speed rotors

The needs of the generation system6 and the gearbox drive the whole design of a fixed-speed rotor. When wind speeds are not optimal, the efficiency of this design may suffer. The main stream of wind turbines in usage today have fixed pace rotors, however, variable speed rotors are increasing market share [10].

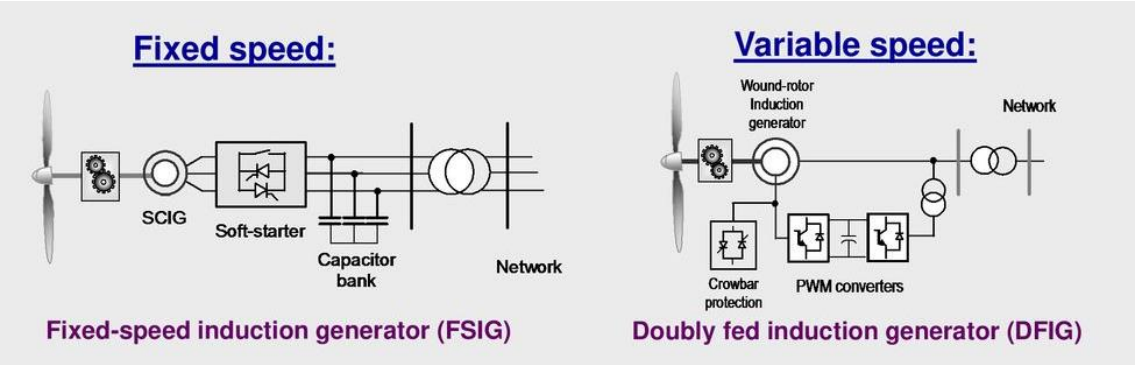

Figure 1.6 Fixed speed rotor and Variable speed rotor [13]

Wind energy can be harnessed more efficiently with variable-speed rotor designs. These further lessen the strain on rotor and other drive train elements. Power electronic converters are required for a turbine to be connected to the grid because variable speed rotors provide varied power output. Power electronic converters convert the electricity generated into the voltage and frequency required for grid distribution. They also make it possible to choose a better versatile generator. Through this additional feature, a low-speed generator may be selected, increasing the variety of locations where these wind turbines can be installed. [10].

The goal of rotor design and analysis is to maximize the power coefficient as a function of the tip-speed ratio (TSR). The TSR is the ratio of the tip-speed of the blade to the inbound wind velocity. This ratio is also closely related to sturdiness, which lowers energy production costs. Consequently, an extended blade has a higher TSR and a faster rotational speed. For a given power output, a higher rotational speed reduces torque on the drive train. That rise in rotational speed, yet, is louder and contributes to blade soiling (The accumulation of bugs and dust on the blade's forefront raises the friction coefficient.) [10].

Wind turbines with Fixed-Speed Induction Generators (FSIG) use a squirrel-cage induction generator that is clearly linked to the system. The slip (and thus the rotor

speed) differs in proportion to the quantity of energy created. The rotor speed fluctuations in these turbines are relatively minimal (one or two percent). Because the induction generator utilizes responsive power, capacitor banks are employed to provide reactive power while also improving the power element. To energize the generator, an intercepting thyristor soft-start unit is employed, then after it's required operational speed is attained, it is circumvented. Overcurrent's are avoided during startup. Pitch control is commonly used to exert power control.

Wind turbine rotors reach their greatest competence at a specific tip speed ratio. The FSIG, on the other hand, revolves at a constant speed. Energy capture can be improved by varying the rotational speed with the wind speed so that the turbine is always running at the optimum tip speed ratio (DFIG machines), or by running the turbine at one of two fixed speeds so that the tip speed ratio is closer to the optimum than with a single fixed speed. If separate generators are needed for each speed of turbine rotation, the two-speed operation is relatively expensive to build. Generators with varying numbers of poles can be attached to gear.

1.4 Problem Statement

The major focus of the wind industry is to improve the designs of large wind turbines. This has led to compromise the small wind turbines and designs of LWTs are adopted for SWTs. There is huge potential for SWTs to produce electricity in urban settings, given that dedicated designs are developed for such applications. Work needs to be done to minimize cut-in speed and starting time.

1.5 Objectives

The goal of this study is to validate the design and performance analysis of the optimized rotor for small wind turbines that is claimed to start relatively quickly without heavy penalties on power outputs. This analysis would help achieve the following major objectives.

- To fabricate the optimized micro-wind turbine of the design proposed in the parent research.
- To perform experiments to identify power outputs at different tip speed ratios.
- To observe the starting time and cut-in speed of the optimized micro-wind turbine.

- To perform experiments to identify rotational speed at different tip speed ratios.

1.6 Scope of Work

The parent research of this investigation has developed and analyzed the performance of a new optimized micro-wind turbine that is approved by computational analysis for fabrication. Therefore, this research work attempts to present the prototyping and experimental analysis of the optimized micro-wind turbine. Various indoor experiments were designed and conducted in a controlled environment to access the performance of the optimized micro-wind turbine to achieve desired tip speed ratio.

Summary:

This chapter discusses the background of energy demand and usage. In the beginning consumption of different energy resources is discussed. After that global and Pakistan's wind energy scenario is discussed. A later little background of wind turbines and types of wind turbines are discussed. At the end of the first chapter problem statement, objectives, and scope of this work are discussed.

List of References:

[1] S. Dale, Statistical Review of World Energy 2021, 2021. https://www.bp.com/en/global/corporate/energy-economics/statistical-review-of-world-energy.html.

[2] P. de Almeida, P.D. Silva, The peak of oil production—Timings and market recognition, Energy Policy. 37 (2009) 1267–1276. https://doi.org/10.1016/J.ENPOL.2008.11.016.

[3] EIA, The international energy outlook 2009 (IEO2009), 2009.

[4] J.G. Leishman, Principles of Helicopter Aerodynamics, Cambridge University Press, 2016. https://books.google.com.pk/books?id=uscAMQAACAAJ.

[5] S.N. Akour, M. Al-Heymari, T. Ahmed, K.A. Khalil, Experimental and theoretical investigation of micro wind turbine for low wind speed regions, Renew. Energy. 116 (2018) 215–223. https://doi.org/10.1016/J.RENENE.2017.09.076.

[6] World Wind Energy Association, Wind Power Capacity Worldwide Reaches 597 GW, 50,1 GW added in 2018 - World Wind Energy Association, (n.d.). https://wwindea.org/wind-power-capacity-worldwide-reaches-600-gw-539-gw-added-in-2018/ (accessed October 11, 2021).

[7] W.W.E. Association, Wind Power Capacity reaches 546 GW, 60 GW added in 2017 - World Wind Energy Association, (2017). https://wwindea.org/2017-statistics/ (accessed October 11, 2021).

[8] G.M. Joselin Herbert, S. Iniyan, E. Sreevalsan, S. Rajapandian, A review of wind energy technologies, Renew. Sustain. Energy Rev. 11 (2007) 1117–1145. https://doi.org/10.1016/J.RSER.2005.08.004.

[9] P.D. Clausen, D.H. Wood, Recent advances in small wind turbine technology, Wind Eng. 24 (2000) 189–201. https://doi.org/10.1260/0309524001495558.

[10] J.G. McGowan, S.R. Connors, WINDPOWER: A Turn of the Century Review, Annu. Rev. Energy Environ. 25 (2000) 147–197.

https://doi.org/10.1146/annurev.energy.25.1.147.

[11] J. Ball, Wind Power Hits a Trough - WSJ, (n.d.). https://www.wsj.com/articles/SB10001424052748704629104576190812458488694 (accessed October 11, 2021).

[12] D. Nigam, What are Vertical Axis Wind Turbines (VAWTs)?, (2019). https://blog.arborwind.com/what-are-vertical-axis-wind-turbines (accessed October 11, 2021).

[13] B. Mccaffrey, Wind Turbine Technology Overview, n.d. https://slideplayer.com/amp/13787336/ (accessed October 11, 2021).

Chapter 2 Literature Review

2.1 Introduction

Wind energy technology has improved tremendously in the last several decades as it has grown in importance and popularity as a green energy source. As the most prominent wind turbine aerodynamic model, the Blade Element Moment Theory (BEMT)-based approach/method has been intensively explored and generally acknowledged to be tolerably effective in wind turbine design and analysis. The Computational Fluid Dynamics (CFD) based technique/method has lately demonstrated to be a feasible alternative prospective solution for wind turbine aerodynamics with the progress of powerful computing technology.

2.2 Blade Element Momentum Theory (BEMT)

The BEM methodology is the combination of momentum theory and blade element momentum theory. It is also called as strip theory [1], resulting in the standard theory of wind turbine rotor aerodynamics. Blade is divided into multiple annular components. One dimensional linear momentum model is applied to every annular element. Forces and power are estimated and combined founded on the sectioned airfoil lift and drag coefficients, chords, and twist angles of the blade geometry. Wind tunnel measurements are often used to get information on aerodynamic characteristics of airfoils such as lift drag and moment coefficients.

2.2.1 Key Points of BEMT

The induction factors and airfoil aerodynamic characteristics are two critical elements in the BEMT for successful application.

- Model of wake induction; The BEM technique defines axial and tangential induction factors to characterize the axial and tangential induced velocity (see Appendix A for definition). For both on- and off-design analysis, the two induction factors are necessary to calculate the total power coefficient.
- Coefficients of lift and drag; The BEM approach demands the description of aerodynamic properties of airfoils at both low and high angles of attack. The amount of power produced varies according on lift and drag measurements.

2.2.2 Advantages and Limitations

Many researchers agree that the BEM method is the most widely used and efficient method for designing and analyzing wind turbine blades [2]. Its benefits are as follows:

(1) All aerodynamic concerns have been defined and resolved using critical techniques, in conjunction with mean amounts produced for every ingredient. As a result, the completion time is reduced.
(2) The lift, drag, and moment coefficients represent the profile of an airfoil. It is adaptable in terms of applying the aerodynamic properties of an airfoil to various wind turbine blades.
(3) The chord and twist angle distributions of the blade are directly related to the power coefficient. As a result, the BEM method can be used in any code, including aeroelastic codes. Automatic global optimization is possible when combined with advanced search algorithms.
(4) Because it is not essential to solve the detailed flows, it consumes fewer processing resources.
(5) It has a good track record and is reasonably accurate.

As a result, it has been widely researched and used in the modeling of wind turbine blades. Several techniques and procedures have been established to determine the ideal chord and twist angle divisions, as well as to evaluate rotor power and aerodynamic presentation. Trendy wind energy shape and evaluation algorithms such as GH-Bladed, AeroDyn, WT Pref, and others were all founded on fundamental BEM theory. Many in-house codes have been developed and changed to meet the unique requirements of businesses, research organizations, and universities. Malawi presented a method for calculating the optimal relative wind angle offered a rotor diameter and sturdiness [3,4]. Vitale created a program to determine optimal blade structure for HAWT while maximizing rotor power efficiency [5]. The BEM method is widely used in the design and study of wind turbines. However, there is much debate in the scientific community over the BEM method's limitations.

Even if the BEM concept has been extensively employed for wind turbine blade layout with satisfactory precision and effectiveness in pre-freeze relentless streams, the influence of actual three-dimensional flow in equally balanced and unstable (i.e., stop) situations has to be researched. Many types of research indicated that the BEM

technique is inaccurate in turbulent wake circumstances and underestimates loads and energy production in shut down circumstances [1]. These are largely connected to the fundamental hypotheses: in momentum theory, the shift in the air cascade at any given time is exclusively attributed to the disc's push. When the turbine is working at elevated wind rates, the downstream enlarges significantly and is plagued with tumult and recirculation. This complicated flow is no longer described by momentum theory. Furthermore, there is no stream transmission between annular blade components, according to blade element theory. To put it another way, the annular tubes are impenetrable. Flows in distinct annular tubes tend to interact, resulting in three dimensional streams such as width-wise streams. The two primary restrictions for un-yawed situations are as follows:

1) Failure under situations of the tumultuous wake

According to momentum theory, the flow velocity far downstream is U(1-2a), where U is the natural upstream velocity and an is the axial induction factor. When a0.5 is reached, the rate of the further downstream develops minus, that is illogical. Under heavy-loaded situations, the BEM theory is unable to capture the connection amongst the propulsion factor and the axial induction components.

2) Under-prediction in stall situations

The influences of the blade components are described through the airfoil's raise and friction coefficients in the BEM method. The statistics are collected through 2D wind tunnel analysis or may be created using computational algorithms e.g. EPPLER [6] and XFOIL [7]. Techniques that depend solely on 2D flow characterizations have been demonstrated to be incapable of modelling complicated 3D flows [8]. Flow details show that blade rotation changes the pressure dissemination on the exterior of blade, that can result in advanced uplift and lesser friction when evaluated to 2D aerodynamic information and 3D stall-interruption under halt circumstances [9]. The lift coefficients (Cl) of a rotating wing are significantly higher than those of a stationary wing at high angles of attack, as measured in a wind tunnel. As a result, stationary airfoil characteristics from wind mill tests are incapable of correctly predicting power output at high angles of incident. Himmelskamp initially observed this phenomena in helicopter propellers in the 1940s. Himmelskamp [10], on the other hand, noticed no increase in drag. Because the stall angle is delayed, many researchers naturally reduce

the drag coefficient [9]. The observed pressure distributions revealed that the blade root part had higher lift and drag coefficients than the blade tip [10]. In terms of power generation, it was frequently demonstrated that the wind turbine rotor power exceeded the. At elevated wind rates, values for halt-controlled turbines were derived using stationary coefficients. Many scientists refer to this as "halt-interruption" or "revolving properties" in wind turbine aerodynamics [11] [12].

Despite the fact that the BEM technique is precise and cost-effective to blade shape and evaluation under model circumstances, off-shape aerodynamics remains a mystery. Due to W1Solved constraints in specifying the axial induction factor in severely loaded settings (high wind rates, low TSRs), sculpting the halt interruption phenomena, and so on. The best blade design is only beneficial in certain situations. When the wind speed varies, the turbines do not operate at their optimal intended settings. As a consequence, the turbine may operate in both on-design and off-design modes throughout the year at a wide variety of wind speeds. Furthermore, data employed in wind turbine design and analysis for airfoils is frequently insufficient. These figures are based on 2D wind turbine measurements (2D). These tryouts are time-ingesting and costly. Airfoil testing at elevated angles of incient is not practicable due to excessive vibration and a high level of uncertainty. As a result, anticipating validated results across a broad range of Reynolds numbers is unrealistic. Furthermore, the behavior of an airfoil in two-dimensional (2D) stationery and tunnel testing is markedly different from that of three-dimensional (3D) spinning blades. The vortex formations that surround a revolving wind turbine blade are far more complicated than the wind tunnel-tested wing model.

2.3 Computational Fluid Dynamics

A deeper knowledge of 3D flow physics is required to quantify the empirical elements that underpin the BEM approach [13]. The computational fluid dynamics (CFD) method is an alternate methodology for studying the rotor aerodynamics of a wind turbine. CFD solves the fluids' differential governing equations accurately and numerically. The mathematical model for a fluid dynamic issue is based on the continuity, momentum, and energy conservation equations. These derivative equations are known as Navier-Stokes equations [14,15]. A locked-structure (tumult prototype) of the controlling calculations is developed and deciphered time-feebly, beside

supplementary flexible passage equations or pragmatic viscosity calculations. A physical problem may be effectively handled by applying complicated key arrangements and turbulence simulations, which provide a minimal but precise explanation of periphery situations as well as excellent discretization of the fluid volume of interest. The job is typically accomplished in 3 stages: pre-handling, solution, and post-handling. These steps can be completed individually in one or more subroutines.

With the rapid development in computer power, the Reynolds Averaged Navier Stokes computational fluid dynamics approach was widely used in the engineering and scientific sectors to explore three dimensional streams across a blade. The RANS-based CFD technique is likely to be used in the wind energy sector shortly [15]. This section discusses the essential features of the RANS CFD method, as well as the present status and challenges of this methodology in aerodynamic study of turbines.

2.3.1 Key Points of CFD

Because of the inconsistent nature of the Navier Stokes equations, it is exceedingly difficult to generate a full 3D turbulent flow model of a wind turbine rotor with fine characteristics in a time-dependent manner using methods such as direct numerical simulation (DNS).

Some researchers use large eddy simulation (LES) and detached eddy simulation (DES) methodologies in wind turbine aerodynamics [16]. RANS equations, on the other hand, are most commonly employed to describe the change in flow domain produced by turbulence near wind turbine blades because they are computationally efficient. Three important factors are required to achieve a reasonably accurate solution for wind turbine aerodynamics:

- An excellent mesh quality
- An improved turbulence model
- A precise solution scheme

The meshing stage is the most interactive and time-consuming of the three components listed above. There are numerous existing models for turbulence modeling available, as mentioned below. The computer solves the problem, which is often accomplished

through the use of a paid industrial programs e.g., Fluent, CFX or by changing current code.

2.3.2 Existing Situation and Barriers

The current state and issues with predicting wind turbine rotor performance using the 3D CFD approach are covered here.

2.3.2.1 Geometry and Mesh

A precise 3D geometry of the wind turbine rotor in digitized format, generally in "computer-assisted design" (CAD) format, is required to simulate a wind turbine rotor using CFD. The blades of wind turbines are typically twisted and tapered. The blade's sectional airfoil has a slightly curved foremost boundary and a crisp or thin blunt behind boundary. To unravel the boundary layer surrounding the blade sides, the boundary layer mesh must have a high enough resolution. To guarantee a meticulous explanation in the boundary drift, the non-dimensional cell hedge gap Y PLUS ought to be less than or ought to be one. Furthermore, a big sufficient stream area is required to eliminate disruptions from area border planes, and a good abundant record step is preferred to provide a decent result. To obtain an accurate boundary flow solution, the dimensionless cell wall distance Y PLUS should be less than or close to one. Furthermore, a big enough flow domain is required to eliminate disruptions from domain border surfaces, and a fine enough time gap is preferred to produce a decent outcome.

In the literature, three types of mesh have been utilized in wind turbine rotor aerodynamics analysis: unstructured mesh, structured mesh, and hybrid mesh [12,17]. Numerous shifting structure mesh and energetic overset mesh topologies have been utilized in many research publications to cope with multi-components in wind turbine rotor aerodynamics modeling. When no yawed streams arise and no module communications are explored, a single frame mesh is commonly utilized to simulate one domain for simplicity.

2.3.2.2 Turbulence and Transition

There are various turmoil prototypes given with promising findings for wind turbine airfoil and rotor aerodynamics study to investigate the flow environment around

spinning wind turbine blades: The Spalart-Allmaras (S-A) model, the conventional k-epsilon (k-) model, the k-omega (k) model, the Shear Stress Transport (SST) k- model, and the transition SST model These models' specifications may be found in [18]. According to Villalpando's study, the SST k- model agrees better with experimental data than other turbulence models such as the S-A model, the k- model, and the Reynolds Stress Model (RSM) [19].

The transition equations (one for intermittency and the other for the conversion momentum width Reynolds number) relate with the SST k- turmoil prototypes in the transition SST model. Because there are two extra transfer equalities concerned, it is clear that the transition model takes more time and is extra receptive to converts than the SST k- theory. Some studies attempted to find a happy medium. Catalano used the SST k- model with an enforced change position that is ten percent downstream from the anticipated idea of a completely turbulent model to conduct a RANS study [20]. The offset, on the other hand, is based on previous experience with this method. The transition SST model was shown to exhibit promising accuracy in forecasting transition flows while not employing forced variables to catch the transition phenomena like turbulence models do [21,22].

Many studies have been conducted on the conversion model. The Menter's conversion model was studied on the 2D S809 airfoil, and better agreements were obtained for angles of attack ranging from 0° to 9°, with the discrepancy at high angles of attack being more likely caused by 3D flow effects than the 2D simulation model cannot represent [23]. Langtry's research produced a full 3D wind turbine rotor using the S809 airfoil, the transition model was reported to be relevant to modern CFD techniques such as non - structured grids and massively parallel execution, and the transition model was claimed to be well suited to predict wind turbine rotor aerodynamics [23]. The same conclusion was reached: Menter's transition model can more precisely forecast the transition and separation, but a longer convergence time is required [24]. Later, the Menter's correlations were enhanced and verified for low Reynolds number external flows, which were reported in 2009 [22]. Even though it takes time to compute, the transition model is said to be sensitive [25,26].

In summary, the transition model can enhance the findings based on 2D airfoil aerodynamic data; transition modeling in 3D under stall circumstances is a

complicated subject that is still being researched. As numerous studies have proven, all RANS models are incapable of modeling stalls at high wind speeds. DES is another method that has been considered. However, the DES technique is tighter and more sensitive to mesh resolution, and it is very computationally costly. Li provided a typical example of this method utilized in wind turbine rotor aerodynamics in 2012 [27]. The DES technique is not feasible in this project due to time and budget constraints. However, utilizing the 3D RANS-CFD approach, specific information such as pressure distribution, torque, moments, and force coefficients along the span-wise direction may be provided, offering a more thorough explanation of the stall phenomena.

2.4 Betz Limit

A German Physicist Albert Betz calculated an expression of maximum theoretical efficiency a wind turbine can achieve. Maximum energy a wind turbine can extract from winds kinetic energy during an open channel flow is known as Betz limit. Albert Betz calculated the Betz limit to be 59.3 [28]. Wind turbines can't exceed the Betz limit in any condition. Wind turbines efficiency is calculated as the percentage of Betz limit. Modern wind turbines can achieve practical efficiency of 80 % of Betz limit [29]. There are numerous practical and design factors that affect the efficiency losses of wind turbines i.e., tip losses, wake effects, mechanical losses, and rotor design losses. There is a simple model called the actuator disk model that helps in calculating the efficiencies of the wind turbine. In this model, the turbine is replaced with a disk. U_t is the velocity of airstream and P_1, P_2 are initial and final pressures Figure 2.1. The equation shows the expression of power produced by the turbine.

$$Power = (P_1 - P_2) A_t U_t \quad (1)$$

$$A_u U_u = A_d U_d = A_t U_t \quad (2)$$

Where A_t represents the disk area of the turbine.

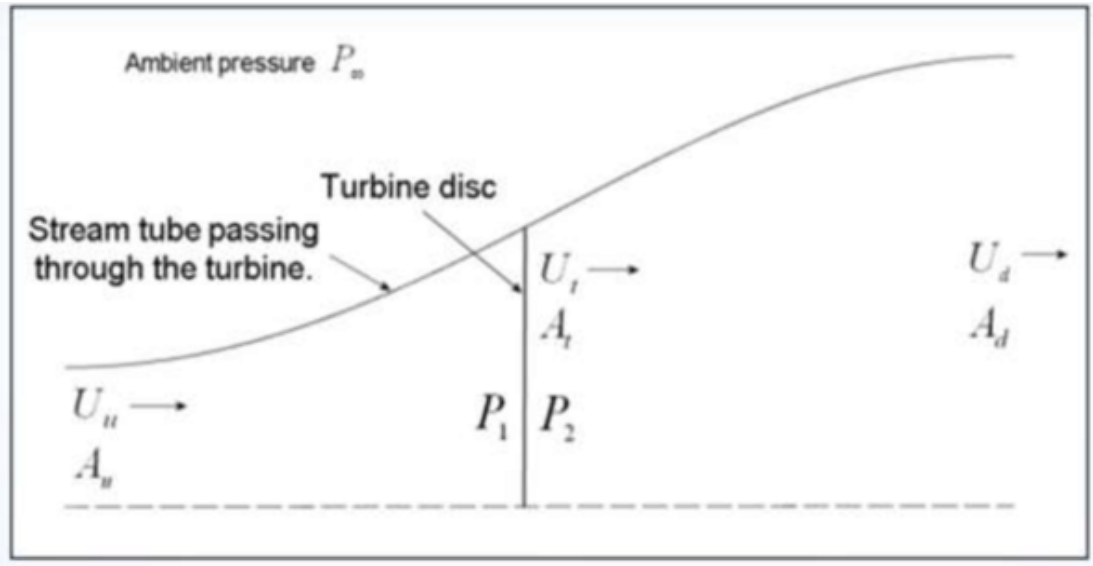

Figure 2.1 Betz Limit Demonstration [30]

Momentum theory says momentum difference between the upstream and downstream flow of disk equals the force applied on the wind turbine.

$$(P_1 - P_2)A_t = Mass\ flow\ \times Velocity\ difference = \rho A_u U_u (U_{u-} U_d) \tag{3}$$

$$P_a + \frac{1}{2}\rho U_u^2 = P_1 + \frac{1}{2}\rho U_t^2 \tag{4}$$

$$(P_1 - P_2) = \frac{1}{2}(U_u^2 - U_d^2) = \rho \frac{A_u}{A_d} U_u (U_u - U_d) = \rho U_t (U_u - U_{d)} \tag{5}$$

$$U_t = \frac{1}{2}(U_u + U_d) \tag{6}$$

$$\eta = \frac{Power}{\frac{1}{2}\rho A_t U_u^3} = \frac{1}{2}(1 - \frac{U_d}{U_u})(1 + \frac{U_d}{U_u})^2 \tag{7}$$

Where U_u, U_t, and U_d are the air velocity at the inlet, turbine disk, and outlet respectively. ρ, represent air density. P_a represents the atmospheric pressure both upstream and downstream of the turbine disk. Figure 2.2 shows the efficiencies are varying with the ratio of downstream and upstream velocity. Data used in figure 2.2 was taken from [31]. Equation 4 tells us that the maximum efficiency is achieved at $U_d/U_u = 1/3$ where $A_d/A_u = 3$ and efficiency (η) becomes 59.3 %.

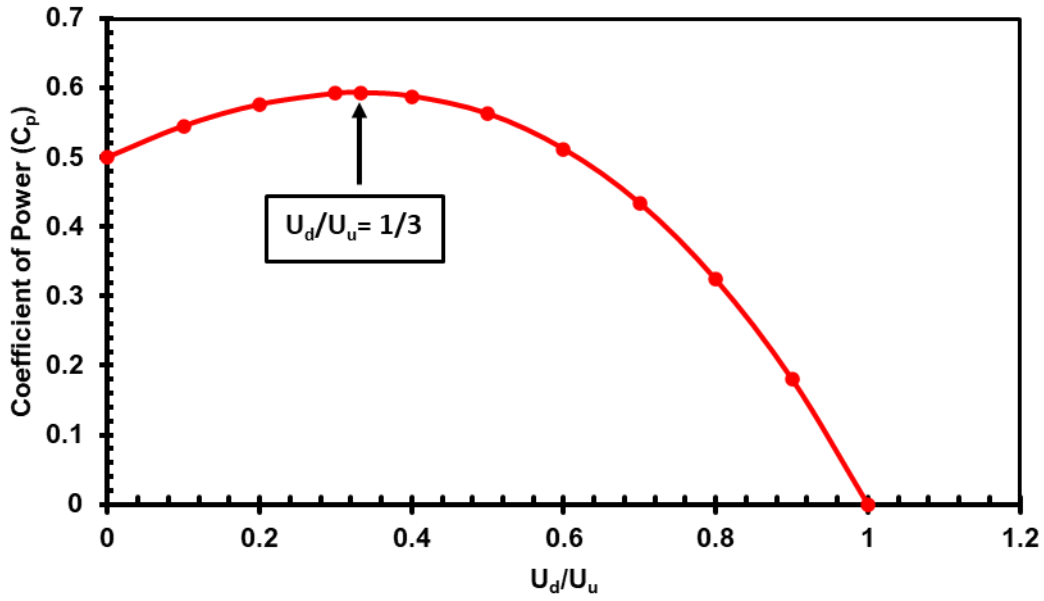

Figure 2.2 Coefficient of Power Curve wrt. U_d/U_u

2.5 Small Wind Turbine (SWT)

Small wind turbines are used for the microgeneration of electricity. They can produce up to 50 KW power. Majorly SWT systems are made based on HAWT. SWT is not as efficient as large wing turbines (LWT), but they are beneficial in several ways. SWT is categorized into three types [32].

- Micro Wind Turbine (1-5 KW)
- Mid-Range Wind Turbine (5-20 KW)
- Mini Wind Turbine (20-50 KW)

In recent years SWTs have received a lot of attention. Researchers have worked on numerous aspects of SWTs to make them efficient and commercially more viable. Devashish et al proposed a new computational approach for blade design and performance investigation of SWTs. Their design is effectual as it varies the angle of attack of the blade and hence generates maximum power even in low wind conditions. They used SG6043 airfoil and emphasized the SWTs over multiple tip speed ratios to investigate the performance of SWT [33]. They achieved a maximum C_p of 0.54. Figure 2.3 shows the C_p curve of the wind turbine.

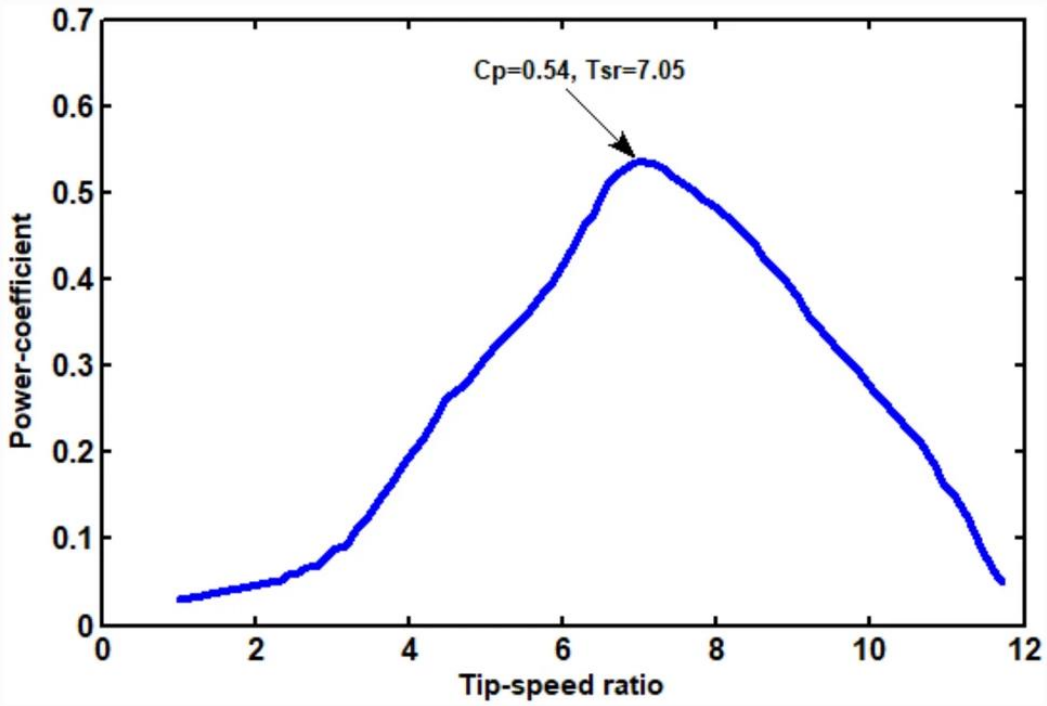

Figure 2.3 Coefficient of Power Curve [33]

Samuel et al worked on the fatigue spectra of SWTs. They used the load model to find the fatigue life of SWTs. Based on the premise that the major fatigue load is the gyroscopic bending moment at the blade root during yaw, they presented a straightforward approach for estimating the fatigue spectra of passively operated small wind turbines [34].

Yasser et all simulated an SWT blade made of reinforced glass fiber polypropylene nano composite. They reported that bias and deflection can be reduced by adding multiwalled carbon nano tubes in the reinforced glass fiber polypropylene and chopped polypropylene glass respectively. Figure 2.4 shows blade deflection at TSR 7.0 for different materials used in their work. [35].

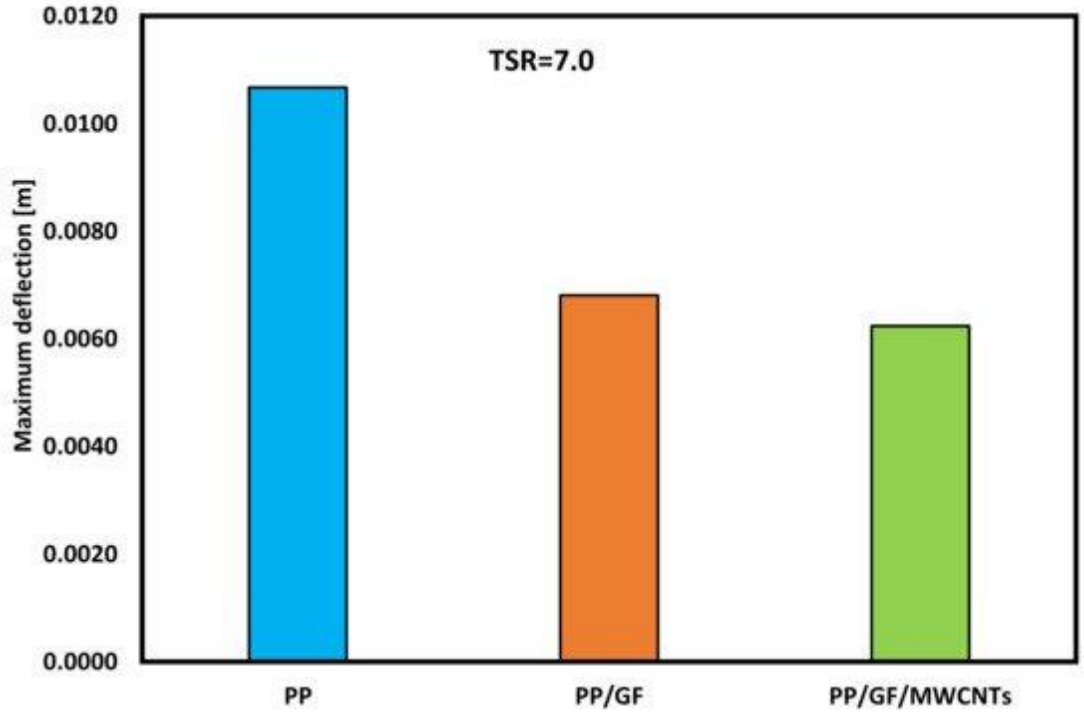

Figure 2.4 Blade Deflection at TSR=7 for different materials'

2.5.1 Advantages of Small Wind Turbines

SWT can produce electricity comparable with LWT and they are less efficient in terms of producing power, but they come in handy in many aspects of practical application. From design to practical installment SWTs are very easy to install and easy to maintain. Major advantages of SWTs include

- Due to their small size SWTs can be installed in a wide range of locations. They can be installed on rooftops in urban and rural areas.
- They have a small cut in speed that means they can start producing electricity in low wind conditions.
- A battery system can be used to store produced energy. In LWTs battery storage systems can’t be used.

Summary:

Chapter two includes the literature review relevant to our work. In the literature review, we started with the discussion of different approaches that can be used to design a wind turbine i.e., BEMT and CFD. BEMT and CFD are discussed in detail after that. Key elements, advantages, and limitations of BEMT and CFD are covered in detail in this chapter. After that Betz limit is discussed in detail to give the idea about the practical and theoretical efficiency. After that small wind turbines and their types are discussed. To conclude the chapter advantages of SWTs and some previous work is discussed

List of References:

[1] J.F. Manwell, J.G. McGowan, A.L. Rogers, Wind Characteristics and Resources, in: Wind Energy Explain., Segunda, 2010: pp. 23–89. https://doi.org/10.1002/9781119994367.ch2.

[2] K. Ameku, B.M. Nagai, J.N. Roy, Design of a 3 kW wind turbine generator with thin airfoil blades, Exp. Therm. Fluid Sci. 32 (2008) 1723–1730. https://doi.org/10.1016/J.EXPTHERMFLUSCI.2008.06.008.

[3] K.Y. Maalawi, M.A. Badr, A practical approach for selecting optimum wind rotors, Renew. Energy. 28 (2003) 803–822. https://doi.org/10.1016/S0960-1481(02)00028-9.

[4] K.Y. Maalawi, M.T.S. Badawy, A direct method for evaluating performance of horizontal axis wind turbines, Renew. Sustain. Energy Rev. 5 (2001) 175–190. https://doi.org/10.1016/S1364-0321(00)00017-4.

[5] A.J. Vitale, A.P. Rossi, Computational method for the design of wind turbine blades, Int. J. Hydrogen Energy. 33 (2008) 3466–3470. https://doi.org/10.1016/j.ijhydene.2008.04.054.

[6] D.M. Somers, J.L. Tangler, Wind Tunnel Test of the S814 Thick Root Airfoil, J. Sol. Energy Eng. 118 (1996) 217–221. https://doi.org/10.1115/1.2871781.

[7] XFOIL, XFOIL, subsonic airfoil development system, (n.d.). https://web.mit.edu/drela/Public/web/xfoil/ (accessed October 12, 2021).

[8] M.C. Robinson, M.M. Hand, D.A. Simms, S.J. Schreck, Horizontal axis wind turbine aerodynamics: three-dimensional, unsteady, and separated flow influences, National Renewable Energy Lab., Golden, CO (US), 1999.

[9] (20) A study on the static stall for horizontal axis wind turbine, (n.d.). https://www.researchgate.net/publication/289108223_A_study_on_the_static_stall_for_horizontal_axis_wind_turbine (accessed October 12, 2021).

[10] C. Lindenburg, Investigation into Rotor Blade Aerodynamics Analysis of the stationary measurements on the UAE phase-VI rotor in the NASA-Ames wind

tunnel, Ecnnl. (2003) 114. http://www.ecn.nl/docs/library/report/2003/c03025.pdf.

[11] D.H. Wood, A three-dimensional analysis of stall-delay on a horizontal-axis wind turbine, J. Wind Eng. Ind. Aerodyn. 37 (1991) 1–14. https://doi.org/10.1016/0167-6105(91)90002-E.

[12] N.N. Sørensen, J.A. Michelsen, S. Schreck, Navier–Stokes predictions of the NREL phase VI rotor in the NASA Ames 80 ft × 120 ft wind tunnel, Wind Energy. 5 (2002) 151–169. https://doi.org/10.1002/WE.64.

[13] J.L. Tangler, J.D. Kocurek, Wind turbine post-stall airfoil performance characteristics guidelines for blade-element momentum methods, 43rd AIAA Aerosp. Sci. Meet. Exhib. - Meet. Pap. (2005) 15583–15592. https://doi.org/10.2514/6.2005-591.

[14] O. Zikanov, Essential computational fluid dynamics, (n.d.).

[15] J. Sumner, C.S. Watters, C. Masson, CFD in Wind Energy: The Virtual, Multiscale Wind Tunnel, Energies 2010, Vol. 3, Pages 989-1013. 3 (2010) 989–1013. https://doi.org/10.3390/EN3050989.

[16] Á. Jiménez, A. Crespo, E. Migoya, Application of a LES technique to characterize the wake deflection of a wind turbine in yaw, Wind Energy. 13 (2010) 559–572. https://doi.org/10.1002/WE.380.

[17] P.K. Chaviaropoulos, I.G. Nikolaou, K.A. Aggelis, N.N. Soerensen, J. Johansen, M.O.L. Hansen, M. Gaunaa, T. Hambraus, H.F. von Geyr, C. Hirsch, K. Shun, S.G. Voutsinas, G. Tzabiras, Y. Perivolaris, S.Z. Dyrmose, Viscous and Aeroelastic Effects on Wind Turbine Blades. The VISCEL project. Part I: 3D Navier–Stokes Rotor simulations, Wind Energy. 6 (2003) 365–385. https://doi.org/10.1002/WE.100.

[18] U.D.F. Manual, ANSYS FLUENT 12.0, Theory Guid. (2009).

[19] M. Reggio, F. Villalpando, A. Ilinca, Assessment of turbulence models for flow simulation around a wind turbine airfoil, Model. Simul. Eng. 2011 (2011).

https://doi.org/10.1155/2011/714146.

[20] P. Catalano, R. Tognaccini, RANS analysis of the low-Reynolds number flow around the SD7003 airfoil, Aerosp. Sci. Technol. 15 (2011) 615–626. https://doi.org/https://doi.org/10.1016/j.ast.2010.12.006.

[21] F.R. Menter, R.B. Langtry, S.R. Likki, Y.B. Suzen, P.G. Huang, S. Völker, A Correlation-Based Transition Model Using Local Variables—Part I: Model Formulation, J. Turbomach. 128 (2004) 413–422. https://doi.org/10.1115/1.2184352.

[22] R.B. Langtry, F.R. Menter, Correlation-Based Transition Modeling for Unstructured Parallelized Computational Fluid Dynamics Codes, Https://Doi.Org/10.2514/1.42362. 47 (2012) 2894–2906. https://doi.org/10.2514/1.42362.

[23] R.B. Langtry, J. Gola, F.R. Menter, Predicting 2D airfoil and 3D wind turbine rotor performance using a transition model for general CFD codes, Collect. Tech. Pap. - 44th AIAA Aerosp. Sci. Meet. 7 (2006) 4643–4653. https://doi.org/10.2514/6.2006-395.

[24] L. Chongming, L. Yuhong, Effects of Turbulence Model and Computational Grid on the Calculation Accuracy of the Aerodynamic Performance of S814 Airfoil Based on RANS, in 2009 Int. Conf. Energy Environ. Technol., 2009: pp. 622–626. https://doi.org/10.1109/ICEET.2009.157.

[25] J.N.N. Counsil, K.G. Boulama, Validating the URANS shear stress transport $\gamma - Re\theta$ model for low-Reynolds-number external aerodynamics, Int. J. Numer. Methods Fluids. 69 (2012) 1411–1432. https://doi.org/10.1002/FLD.2651.

[26] M.R. Ahmed, S. Narayan, M.A. ZULLAH, Y.-H. Lee, Experimental and numerical studies on a low Reynolds number airfoil for wind turbine blades, J. Fluid Sci. Technol. 6 (2011) 357–371.

[27] Y. Li, K.-J. Paik, T. Xing, P.M. Carrica, Dynamic overset CFD simulations of wind turbine aerodynamics, Renew. Energy. 37 (2012) 285–298. https://doi.org/https://doi.org/10.1016/j.renene.2011.06.029.

[28] D.-I.D.A. Betz, The Maximum of the Theoretically Possible Exploitation of Wind by Means of a Wind Motor:, Http://Dx.Doi.Org/10.1260/0309-524X.37.4.441. 37 (2013) 441–446. https://doi.org/10.1260/0309-524X.37.4.441.

[29] T. Burton, N. Jenkins, D. Sharpe, E. Bossanyi, Wind Energy Handbook, Second Edition, Wind Energy Handbook, Second Ed. (2011). https://doi.org/10.1002/9781119992714.

[30] J. Sapra, Aerodynamic Design using Numerical Method (Trapezoidal) for Horizontal axis wind turbine (HAWT) Blade with CAD Model, 2018. https://doi.org/10.13140/RG.2.2.29538.38080.

[31] M. Ragheb, A.M. Ragheb, Wind Turbines Theory - The Betz Equation and Optimal Rotor Tip Speed Ratio, Fundam. Adv. Top. Wind Power. (2011). https://doi.org/10.5772/21398.

[32] British Standard, Wind turbines — Part 2: Design requirements for small wind turbines, 61010-1 © Iec2001. 2006 (2006) 13.

[33] D. Jha, M. Singh, A.N. Thakur, A novel computational approach for design and performance investigation of small wind turbine blade with extended BEM theory, Int. J. Energy Environ. Eng. 2021 123. 12 (2021) 563–575. https://doi.org/10.1007/S40095-021-00388-Y.

[34] S. Evans, S. Dana, P. Clausen, D. Wood, A simple method for modeling fatigue spectra of small wind turbine blades, Wind Energy. 24 (2021) 549–557. https://doi.org/10.1002/WE.2588.

[35] Y. Elhenawy, Y. Fouad, H. Marouani, M. Bassyouni, Simulation of Glass Fiber Reinforced Polypropylene Nanocomposites for Small Wind Turbine Blades, Process. . 9 (2021). https://doi.org/10.3390/pr9040622.

Chapter 3 Methodology

3.1 Case Study

The previously mentioned numerical studies show how computational approaches are vital to the SWTs. Hence the design team of the optimized micro-turbine also performed a CFD study to analyze the performance of the proposed novel design. The CFD study validated the optimized design with a weight factor of 0.7 as the starting time of this blade was 29.7% better than that of the blade optimized for maximum power only. Steady-state simulations were performed for the blade only by employing the sliding mesh technique. The blade was considered a wall (no-slip condition). It was considered as a solid, on which fluid experiences zero acceleration/velocity and create shear stress cross the fluid across the domain, and creates turbulence, which needs to solve according to some created turbulence models. There are several turbulence models.

The comparison of the Cp vs TSR is shown in Figure 3.1, where the power curve predicted by the CFD lags 25% by the design point claimed by the BEMT analysis of the blade design. The BEMT model would not account for the tip losses and secondary flows at the hub, whereas the CFD model would consider these losses. Hence the mismatch of the power curve is evident. The 6DOF simulations were also carried out to analyze the starting time of the blade selected for the numerical investigation.

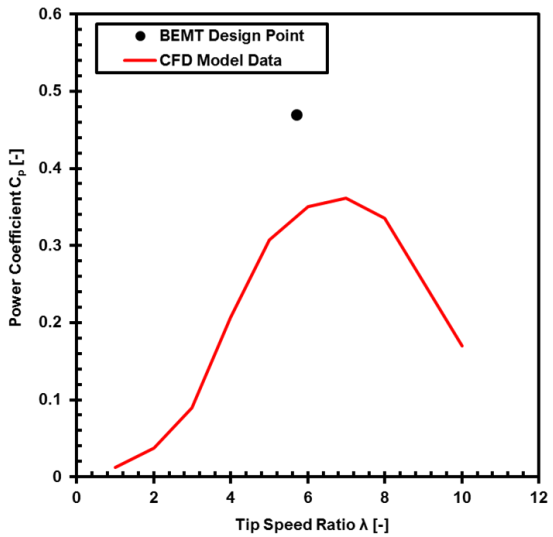

Figure 3.1 Caparison of Cp for BEMT and CFD

At various incoming flow speeds, the starting time was monitored by observing the coefficient of the moment. For wind speed of 5 m s^{-1}, the moment coefficient is shown in Figure 3.2. These graphs show the starting time of the optimized blade is appreciable. The starting time for the optimized case was 2.8 s. Thus, the low cut-in speed and considerable power outputs over a range of TSR are promising. Hence, it suggests proceeding with the design for experimental investigations.

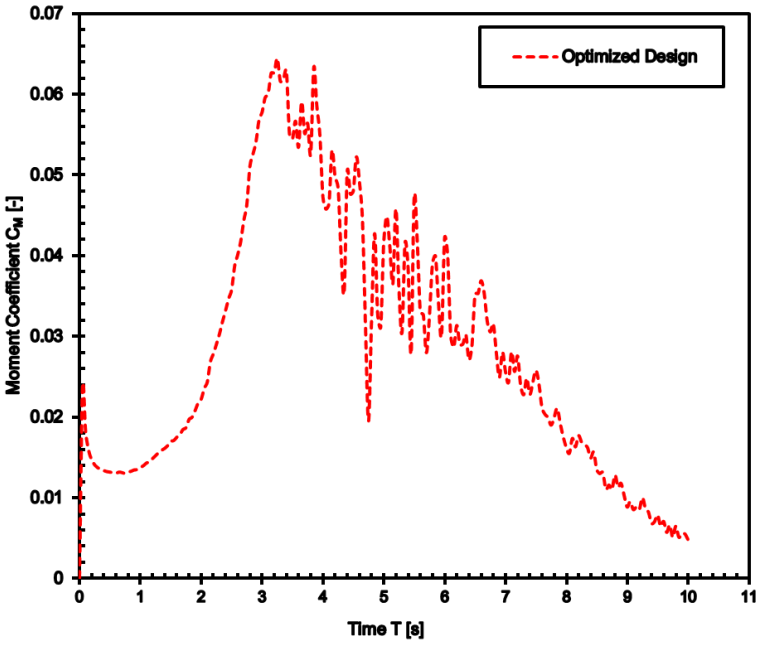

Figure 3.2 Moment coefficient at 5 m s^{-1}

The fabrication of the designed blades of the micro-wind turbine is the most critical part of this research. The novel optimized blade design by Abolfazl et al [5] was used in this research. This design is a complicated 3D structure, made from a unique airfoil and is twisted significantly to obtain the desired performance. This design doesn't include the hub, controller, and generator. Therefore, a small wind turbine system is required which is compatible with the designed blade's shape and inertial properties. A Chinese model, Wuxi 200S2, of a small wind turbine was procured. This wind turbine has a rated power of 200 W, but the designed blade span is rated 1 KW. The selection of wind turbines was done purely based on the lack of availability of huge research funds. After the procurement, the pre-evaluation of the wind turbine was done. This chapter will discuss all the methodology steps in detail that were involved in this work. Figure 3.3 shows a simple flow chart of all the steps used in this work.

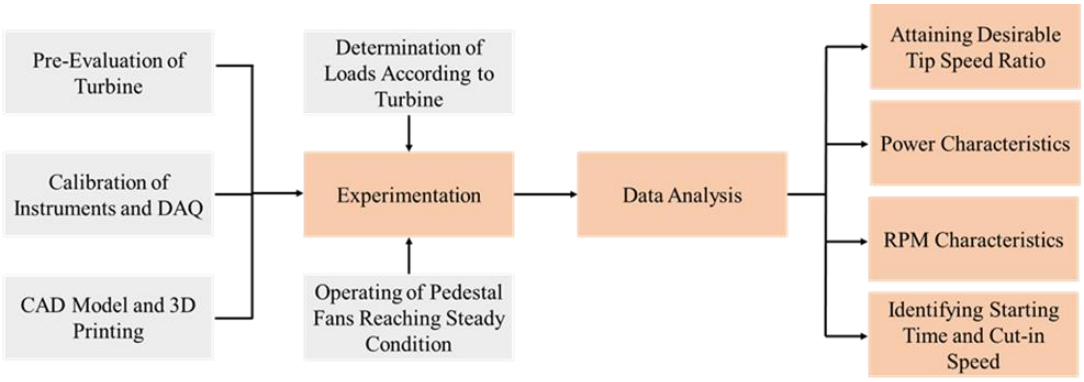

Figure 3.3 The methodology for experimentation

3.2 Pre-Evaluation of wind Turbine

Analyzing the mechanical and electrical properties of a wind turbine is very crucial before any experimentation. The induction generator should be producing the required voltage and the rotor should be able to achieve the desired rpm to proceed with the experimentation. All the features of the acquired wind turbine are listed in Table 3.1.

Table 3.1 Feature of Wuxi Wind Turbine

Parameters	Value
Model	200S2
Rated Power [W]	200
Maximum Power [W]	300
Rated Voltage [V]	12
Rated Wind Speed [ms^{-1}]	11.5
Number of Poles	10
Number of Blades	3
Start-up Wind Speed [ms^{-1}]	2
Wind Wheel Diameter [m]	1.25
Survival Wind Speed [ms^{-1}]	50
Blade Length [mm]	520
Generator	3 Phase Permanent Magnet Synchronous

3.2.1 Electrical Properties

For the validation of the electrical properties of a procured wind turbine, output voltage and the number of poles were measured.

3.2.1.1 Output Voltage

To measure the output voltage of procured wind turbine, it was spun manually with the same blades it came equipped with. The wind turbine rotor was given an artificial rotation using a drill to a certain rotation per minute (rpm). RPM was measured using a lab-scale Tachometer and output voltage produced by the wind turbine was measured using a multimeter Uni-T Model UT203. All the phases of the induction generator were producing 11.8 V.

3.2.1.2 Number of Poles

After that number of poles of a wind turbine was calculated. The number of poles is required to calculate the rpm of the wind turbine. In the previous step, rpm were measured using a tachometer because rpm/synchronous speed is an unknown variable in the formula of several poles. Several remains the same but rpm may vary, and rpm depends on frequency (f) that changes throughout the operation. Therefore, rpm was measured using a tachometer to calculate several poles and after that, we can use this number of poles to calculate rpm whenever we need it as the number of poles doesn't change throughout the operation of the wind turbine. Frequency was given by the data acquisition system (DAQ). DAQ used in this research was from National Instruments model 783338-01DLM. Equation (1) is used to calculate the number of poles. Using this equation, we found the number of poles to be 10. Equation (2) is the same equation rearranged in the form of rpm(N).

$$P = \frac{2 \times 60 \times f}{N} \tag{8}$$

$$N = \frac{2 \times 60 \times f}{P} \tag{9}$$

Where P represents several poles, f represents frequency (Hz) and N represents rpm of the wind turbine.

3.2.2 Mechanical Properties

The procured wind turbine doesn't have a base. Therefore, to operate the turbine and to perform experimentation we need to have a solid base to enhance and make sure the mechanical strength of the wind turbine. A GI pipe of 2.25 in diameter was used as a

pole. The bottom of the pipe was fixed in concrete. Another GI pipe of 2 in diameter was inserted in that pipe to make the height of the wind turbine adjustable. To mount the turbine on the base a flange was needed. To make the flange a stainless-steel plate of 1 cm thickness was taken and was transformed into a round shape using a lathe machine. Four holes were drilled in the flange according to the turbine. Figure 3.4 illustrates the fabrication of flange from stainless-steel plate to final form.

Figure 3.4 Fabrication of Flange

3.3 Configuration of Instruments

Before starting any experimentation configuration of the instruments e.g., DAQ and Anemometer are crucial.

3.3.1 Data Acquisition System (DAQ)

DAQ from national instruments model 783338-01DLM was used in this research. A voltage measuring card and a current measuring card were installed in DAQ to convert the analog signal into a digital signal. To calibrate DAQ LabView software was used. A code was developed to measure power output, mechanical frequency, and period. Figure 3.5 shows a picture of the DAQ system where voltage and current cards are installed. Mechanical frequency measured by a data logger using voltage signal was used in the calculation of several poles.

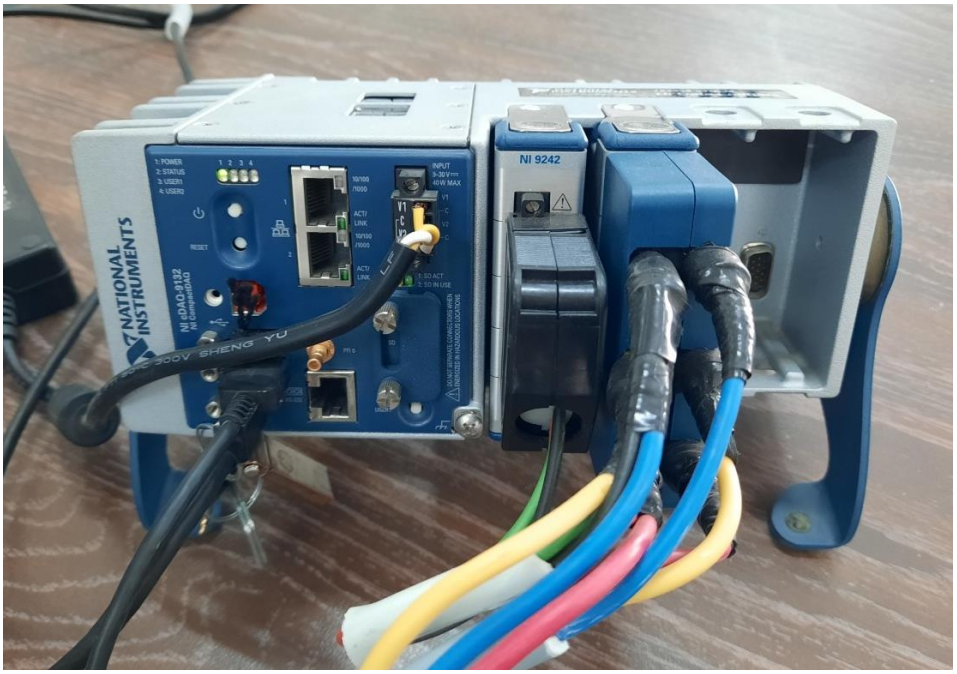

Figure 3.5 Data Acquisition System

3.3.2 Anemometer

An anemometer from Amprobe model TMA 10A was used to measure the wind speed generated from the pedestal fan. As pedestal fans were used to run wind turbines and they don't have any digital speed indication therefore wind speed generated by the fan to rotate the wind turbine blade was measured using the anemometer. Figure 3.6 shows the picture of the anemometer used in this work. It gives the wind speed in m s^{-1}.

Figure 3.6 Anemometer

3.3.3 Tachometer

The tachometer was used to measure the rpm of the rotor. RPM measured by the data logger was compared with a tachometer to account for any error. RPM used in the calculation of several poles was measured by a tachometer.

3.4 Blade Manufacturing

The fabrication of the designed blades of the micro-wind turbine is the most critical part of this research. The novel optimized blade design proposed by Abolfazl et al [5] is a complicated 3D structure as it is built from a unique airfoil and twisted significantly to fulfill the desired performance. However, this design does not include the hub, controller, and generator designs. Therefore, it is required to identify an existing micro-wind turbine system that is compatible with the shape and inertial properties of the proposed new blades. As the initial step a Chinese model, Wuxi, of a micro-wind turbine was procured. The selection was subject to the availability of research funds and hence the wind turbine purchased is smaller than the proposed new design. The blade span of the desired design is rated for 1 kW and that of the purchased turbine is only 200 W. It is thus required to scale down the blade of the new rotor and design a root section to mount the blade on the hub of the procured wind turbine. The

CAD model of the rotor section and the mounting groove on the hub of the Wuxi wind turbine is given in figure 3.7. Moreover, the fabrication of the scale-down blades and a suitable base and pole are also necessary to account for. These aspects are individually discussed in the following subsections of prototyping.

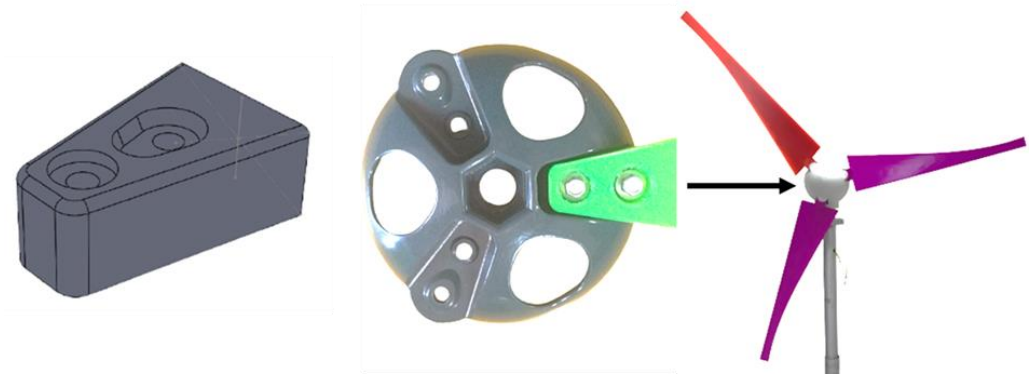

Figure 3.7 The hub with the mounted root of the blade and 3D printed

3.5 Rotor Sizing

The properties and predicted performance parameters of the optimized blade design are given in figure 3.8 below. The optimized design tested for this investigation also considers chord and twist as the optimization parameters. Modifications to the BEMT model were made to cater for the tip losses and used to calculate the power output and starting time of the optimized blade. By using a genetic algorithm to optimize the designs of three SWTs of different power ratings, the parent research claims to achieve both enhanced power and a quick starting time. It is further proposed that a blade design optimized for both power and starting time is desirable for low wind regions. The blade is developed from SG6043 airfoil and is significantly twisted from hub to tip to provide both quick starting time and high-power output. As shown in figure 3.8(a), the optimized blade is twisted by 25^{o} at the root, which drops below 10^{o} at mid-span and eventually reaches just 2^{o} at the tip. Likewise, the ratio of the chord to the blade length is the largest at the root, i.e., 0.2, and steeply drops by more than half at the mid-span. The blade is tapered significantly as the chord to span ratio at the tip of the blade is only 0.05. The BEMT model was solved for 15 sections of the blade to provide power and starting time for inputs of respective twist and chord data of each section. The computer-aided design of the blade is shown in figure 3.8(b). The genetic algorithm was then set to prioritize the two objectives of the optimization by

introducing the weighing factor of power and starting time. On a scale of 0 to 1, the weight factor of 1 was for maximizing the power output only. Likewise, a weight factor of 0.5 would give equal importance to both outputs. Good structural support but still low weight for quick starting time is highly recommended and hence, a material of high strength to weight ratio and the suitable material density is also emphasized by the designers. The weight factor of the blade design considered for this study is 0.7 and the resistive torque is 0.5 Nm. The design promises to produce power just after 2.8 seconds and with the maximum power coefficient of 0.49 at maximum rotation.

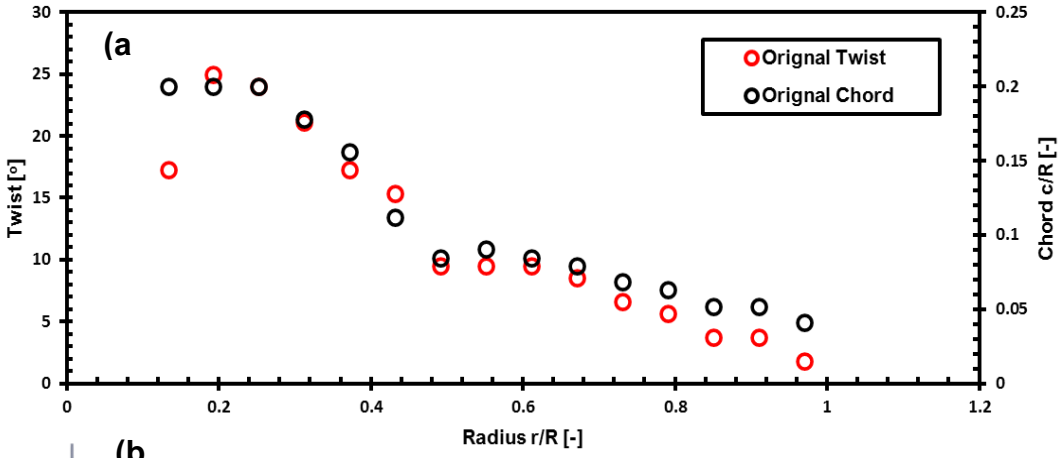

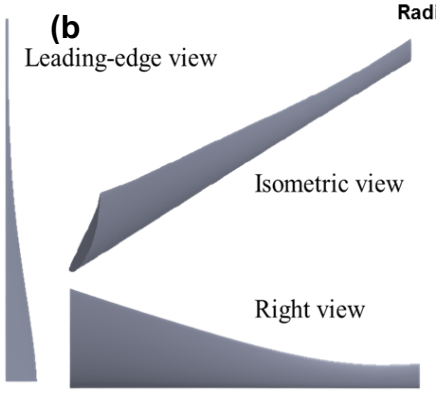

Parameters	Values
Minimum twist [θ_p]	-5°
Maximum twist [θ_p]	25°
Minimum Chord [c/R]	0.01
Maximum Chord [c/R]	0.2
Rated RPM	450
Rated Power [kW]	1
Tip Speed Ratio [-]	5.71

Figure 3.8 (a) Twist and chord distribution of the optimized blade (b) Computer-aided model of the blade (c) Geometric and performance parameters of the optimized small wind turbine

It can be seen in figure 3.9 that the designers would wish to develop a blade of 108 cm to achieve a rated yield of 1 kW. However, the experimental analysis would be performed for a scaled-down wind turbine as is shown in figure 3.9 below. For the blades to affix with the hub of the Wuxi wind turbine, the root section of this blade must be merged with the optimized blade. Moreover, the size of the entire optimized blade is scaled down by a factor of 0.4765 to make it compatible with the 200 W

generator of the Wuxi system. As demonstrated in figure 3.9, the dimensions of the scaled blades are all decreased about the centroid of the actual blade. This would ensure that all the features of the actual blade design will remain intact in shape and the sizes would diminish to the new sizes in the same proportion.

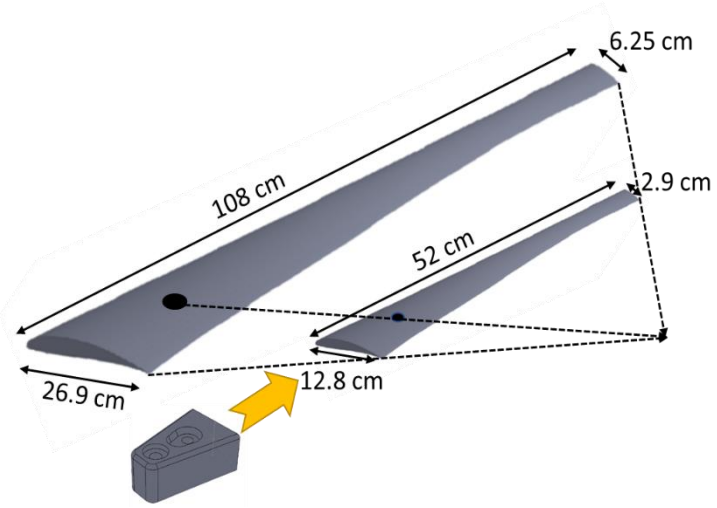

Figure 3.9 The visual demonstration of scaling down the blade and merging the root section.

3.6 3D printing of scaled-down optimized blade

The turbine blades are developed by 3D printing of the scaled-down Computer-Aided Design. Although, the blades could be made of aluminum or wood, which would come at the cost of heavyweight and rough texture, respectively. Hence, the viable approach is to go for 3D printing of the blades. In this case, it is strictly required to match the weight of the printed blades to that of the Wuxi rotor's blades; the moment of inertia of the blades must be the same for both rotors. To this end, the properties of suitable materials for 3D printing are considered, as given in table 3.2 below, and Polylactic Acid (PLA) was chosen for it would provide the mass of the blades as required.

Table 3.2 The properties of the materials for 3D printing of the blades.

Properties	ABS	PLA	PETG	Carbon Fiber
Ultimate Tensile Strength [MPa]	40	65	53	45 till 48
Maximum Service Temperature [°C]	98	52	73	52
Coefficient of Thermal Expansion [$\mu m\ m^{-1}\ °C^{-1}$]	90	68	60	57.5
Density [$g\ cm^{-1}$]	1.04	1.24	1.23	1.3
Extruder Temperature [°C]	220 till 250	190 till 220	230 till 250	200 till 230
Bed Temperature [°C]	95 till 110	45 till 60	75 till 90	45 till 60
Heated Bed	Required	Optional	Required	Optional

The 3D printing facility in the Energy center of NUST was engaged for 48 hours to print each blade. The Inoovo I-fire-XX 3D printer with a testbed of 50x50x50 cm is well equipped to print the blades of our turbine. The testbed and the printed blade are shown in figure 3.10. The rafting approach was utilized for the printing of these blades to ensure strength and meet the mass requirement of the blade. Moreover, rafting was preferred over brimming and skirting for it provides better surface finishing as it is required to reduce the surface drag. The operating conditions for the 3D printing are given in table 3.3 below.

Table 3.3 The specifications of the 3D printing method.

Category	Parameters	Value
Quality	Layer Height [mm]	0.1
	Shell Thickness [mm]	1.2
Fill	Bottom/Top thickness [mm]	1.2
	Fill Density [%]	75
Speed and Temperature	Printing Speed [$mm\ s^{-1}$]	65
	Printing Temperature [°C]	210
	Bed Temperature [°C]	33
Support	Support Type	Entire Blade
	Platform Adhesion Type	Raft
Filament	Filament Diameter [mm]	1.75
	Filament Flow [%}	100
Machine	Machine Nozzle Size [mm]	0.4

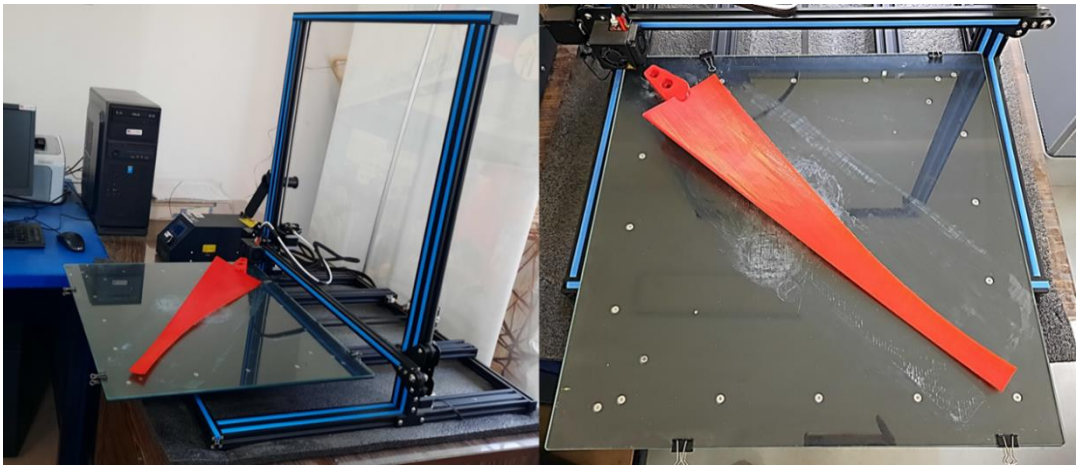

Figure 3.10 The Inoovo i-fire-XX 3D printer and the printed blade.

3.7 Base and Pole

Generally, the pole and base of a small turbine are custom-made by the operators to fit in with the operating conditions and mounting site. The Wuxi wind turbine comes without a pole but with a flange attached to the nacelle of the turbine. Thus, a flange attached with a pole of sufficient height and strength is required to be designed according to the size of the flange attached to the nacelle. The base of the pole also needs to be stable and stationary in high winds to avoid vibrations and distortion in the rotor while it is rotating. These concerns are kept in view to design and develop a pole of metal and a base of reinforced concrete in a plastic bucket. The pole is made telescopic to adjust heigh if needed for experimentation. The flange attached to the pole is a replica of the open provided with the Wuxi turbine; fasteners were available with the purchased turbine.

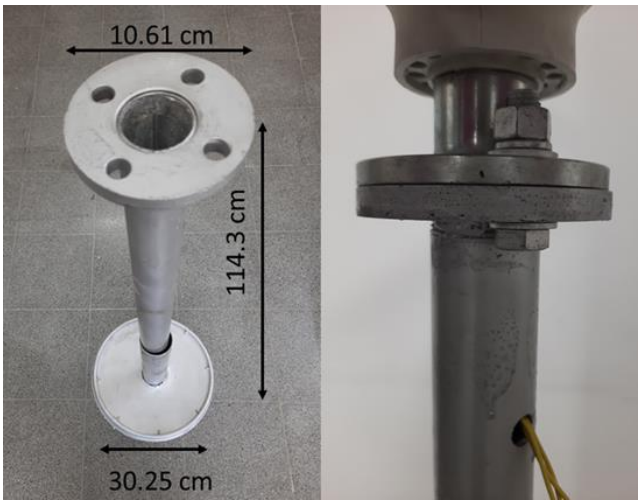

Figure 3.11 Base and Pole (left) Turbine mounted on flange (right)

3.8 Determination of Load According to the Turbine

An electrical load is a component of an electrical circuit that converts current into something useful. A lamp, a resistor, and a motor are among examples. A load is a device that transforms electricity into heat, light, or motion. In other words, an electrical load is the portion of a circuit that connects to a well-defined output terminal.

Circuits include three main types of loads: capacitive loads, inductive loads, and resistive loads. The way they use power in an alternating current (AC) arrangement differs. The load types capacitive, inductive, and resistive are roughly related to lighting, mechanical, and heating loads.

3.8.1 Resistive Loads

Resistive loads are those that include any type of heating element. Incandescent lights, toasters, ovens, space heaters, and coffee machines are examples. A purely resistive load pulls current in a sinusoidal waxing-and-waning pattern in tandem with a sinusoidal fluctuation in voltage – that is, the maximum, minimum, and zero points of the voltage and current values over timeframe up – and contains no additional components.

3.8.2 Inductive Loads

Inductive loads are those that power electric motors. These are found in several home goods and equipment with moving components, including fans, vacuum cleaners, dishwashers, washing machines, and refrigerator and air conditioner compressors. In contrast to resistive loads, current in a fully inductive load follows a sinusoidal pattern that peaks after the voltage sine wave peaks, resulting in out-of-phase maximum, minimum, and zero points.

3.8.3 Capacitive Loads

Current and voltage are out of phase in a capacitive load, as they are in an inductive load. The distinction is that in the case of a capacitive load, the current reaches its maximum value before the voltage. In an inductive load, the current waveform lags after the voltage waveform.

Among the three load types, we used pure resistive load i.e., nichrome wire. Resistive loads were connected in a parallel delta connection.

3.8.4 Output Current

The current produced by the generator is calculated from equation (3).

$$P = \sqrt{3} \times PF \times V \times I \tag{10}$$

$$I = \frac{P}{\sqrt{3} \times PF \times V} \tag{11}$$

$$I = \frac{200}{\sqrt{3} \times 1 \times 12} \tag{12}$$

$$I = 9.66\ A \tag{13}$$

3.8.5 Required Load

The value of the required load to be connected to the three-phase generator was calculated using equation (8).

$$V = I \times R \tag{14}$$

$$R = \frac{V}{I} \tag{15}$$

$$R = \frac{12}{9.66} \tag{16}$$

$$R = 1.25\ \Omega \tag{17}$$

As we have a three-phase permanent magnetic generator so this resistive load of 1.25 Ω should be applied to each phase separately.

3.8.6 Load Calculations

3.8.6.1 1.25 Ω Load

The length of the load 1.25 Ω is very small, the amount of the current withdrawn can melt the wire. Therefore, the loads were made by using loops attached to the ceramic connectors i.e. 10 A.

$$\frac{1}{R_e} = \frac{1}{R_1} + \frac{1}{R_2} + \frac{1}{R_3} + \frac{1}{R_4} \tag{18}$$

$$\frac{1}{R_e} = \frac{1}{5} + \frac{1}{5} + \frac{1}{5} + \frac{1}{5} \tag{19}$$

$$\frac{1}{R_e} = \frac{4}{5} \tag{20}$$

$$R_e = \frac{5}{4} \tag{21}$$

$$R_e = 1.25\ \Omega \tag{22}$$

3.8.6.2 5 Ω Load

$$\frac{1}{R_e} = \frac{1}{R_1} + \frac{1}{R_2} \tag{23}$$

$$\frac{1}{R_e} = \frac{1}{10} + \frac{1}{10} \tag{24}$$

$$\frac{1}{R_e} = \frac{2}{10} \tag{25}$$

$$R_e = \frac{10}{2} \tag{26}$$

$$R_e = 5\ \Omega \tag{27}$$

3.8.6.3 14 Ω and 28 Ω Loads

For these loads 9.66, A current could easily pass through. Wire lengths were taken using a multimeter.

Summary:

This chapter discussed the whole methodology of our work in detail. A flowchart of methodology is attached in the chapter. The chapter starts with a case study of CFD simulation. After that devaluation of the procured turbine is discussed including electrical properties, mechanical properties, the configuration of instruments e.g., DAQ, Anemometer, and Tachometer. After that 3D printing of the blade is discussed. In the end types of loads and calculations of different loads are discussed.

List of References:

[1] J. Ahmad, CFD Evaluation of 1kW Small-Scale Horizontal Axis Wind Turbine for Operations in Low Wind Speed Regions, (2018) 2–7.

[2] N. Nazir, A. Javed, Comparison of 1kw horizontal axis wind turbine rotor blade performance using numerical simulation, 6th Int. Conf. Aerosp. Sci. Eng. ICASE 2019. 2 (2019). https://doi.org/10.1109/ICASE48783.2019.9059224.

[3] D. Marten, J. Peukert, G. Pechlivanoglou, C. Nayeri, C. Paschereit, QBLADE: An Open Source Tool for Design and Simulation of Horizontal and Vertical Axis Wind Turbines, Int. J. Emerg. Technol. Adv. Eng. 3 (2013) 264–269.

[4] A. Betz, The maximum of the theoretically possible exploitation of wind by means of a wind motor, Wind Eng. 37 (2013) 441–446. https://doi.org/10.1260/0309-524X.37.4.441.

[5] A. Pourrajabian, R. Ebrahimi, M. Mirzaei, Applying micro scales of horizontal axis wind turbines for operation in low wind speed regions, Energy Convers. Manag. 87 (2014) 119–127. https://doi.org/10.1016/j.enconman.2014.07.003.

Chapter 4 Experimentation

4.1 Equipment Required

To perform experiments few instruments are required. All equipment used in the experimental setup is listed below. Calibration of some instruments was performed as discussed in chapter 3 and others that don't need calibration were used as it is.

- Wind Turbine
- 3D Printed optimized blade
- DAQ
- Computer setup
- Pedestal fans
- Anemometer
- Wooden board
- Thermal Insulation Board
- Ceramic Connectors
- Resistive Loads
- Circuit breaker
- 3 Core wire
- Mechanical tools
- Multimeter

4.2 Experimental Setup

4.2.1 Turbine and Fans Setup

The experimental setup was made in the machine shed of USPCAS-E NUST. All windows and doors were closed to make to have a turbulence-free environment. We don't want any external wind during the experiment because it can cause turbulence. Obstacle free zone of 10 m peripheries was made to experiment. Four pedestal fans were arranged in a square shape such a way that the total swept area of a fan was 1. 48 m^2. Turbines and fans were arranged in such a manner that wind generated by fans covered the annulus area of the wind turbine i.e., 1.22 m^2. Fans setup was made in a way so that all fans were turned on and off at the same time. The turbine was placed

in such a way that c centroid of four fans was perpendicular to the turbine hub and was 120.3 cm above the ground. Three different points were marked on the ground from the turbine i.e., 80, 140, and 200 cm for wind speed measurement and experimentation. Figure 4.1 illustrates the experimental setup of the turbine and fans. There was no accurate way to change the wind speed from the fans to a substantial value, so the wind turbine was placed on these marks to have different wind speeds. Wind speed was measured at 3 different marks by an anemometer. Five different measurements were taken their average value was accounted for in calculations. The average wind speed measured was 4.6, 4.1, 3.7 m s^{-1} at a distance of 80, 140, 200 cm respectively. Table 4.1 shows the average wind speed at various distances between turbine and fans.

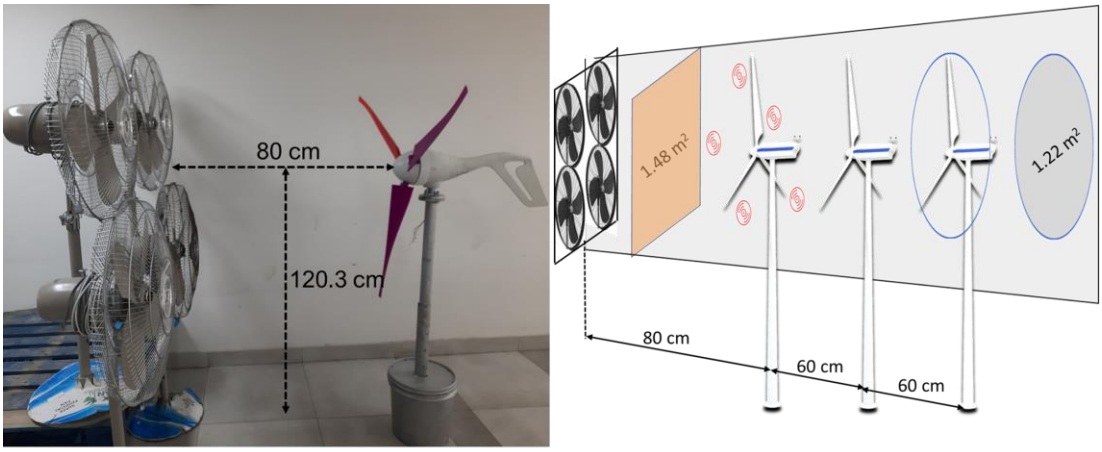

Figure 4.1 Experimental illustration of turbine and fan setup

Table 4.1 Average wind speed at variable distances

Sr. No.	Distance (cm)	Average Wind Speed (m s^{-1})
1	80	4.6
2	140	4.1
3	200	3.7

4.2.2 Circuit Setup

A wooden board was used as a base to make the circuit. A thermal insulation board was used to separate every loop we used to make resistive load prevent short-circuiting and dissipate heat. Thermal insulation was used between loads and a wooden board to prevent any hazards during the experiment. Three resistive loads were connected in

parallel delta connection. 3 core wire is used to get the output current from the turbine. A circuit breaker was installed on each phase. Ceramic connectors were instead of conventional silicon connectors to avoid melting due to heat production during the current passage. From circuit breaker current travels towards DAQ. DAQ processing card measures the current and lets it pass toward loads. DAQ doesn't sense current if the potential is ≤ 0.1 V because current with V ≤ 0.1 V is noise. Figure 4.2 shows the final circuit made for experiments.

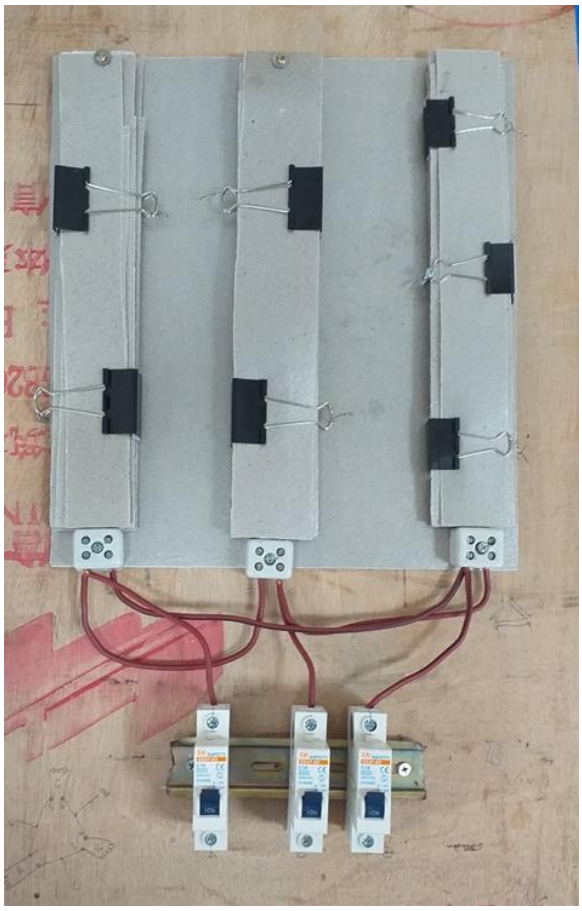

Figure 4.2 Circuit setup

4.3 Computer Setup

DAQ was directly connected to a computer setup (monitor, mouse, and keyboard). During the operation, the monitor displays real-time values of frequency, output power, and the time period and at the same time, it saved all the data. Figure 4.3 shows the overall computer setup connected to DAQ and ultimately to the circuit.

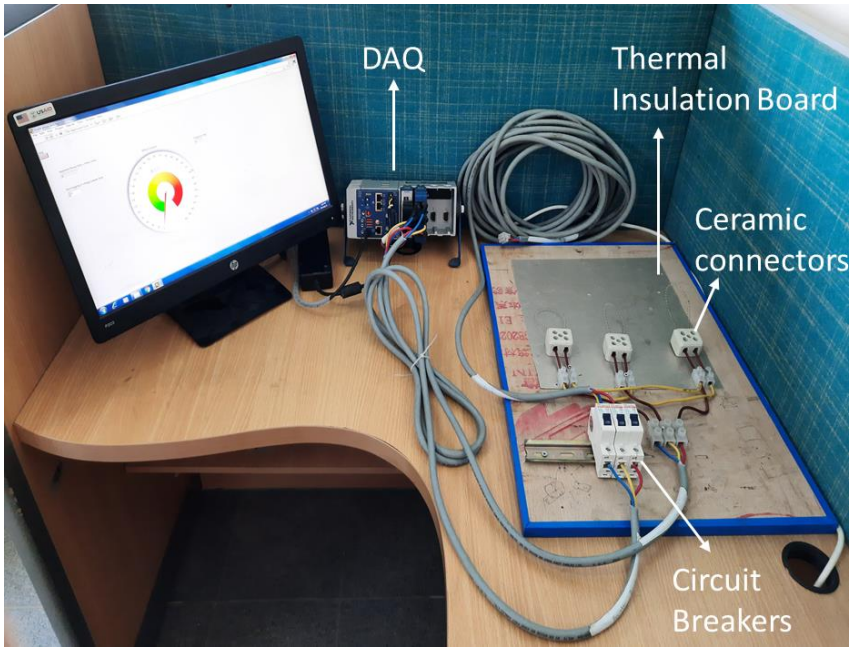

Figure 4.3 Computer setup with DAQ and circuit

4.4 Experimentation

The subject of this research is the experimental assessment of the optimized design of a novel micro-wind turbine in controlled indoor conditions. The experimentation is split into two phases, initially, the acquired Wuxi wind turbine is tested to verify its electric, magnetic, and mechanical fitness in real wind conditions. The second phase is dedicated to testing the 3D printed new optimized design in controlled conditions. In this main experimental part, a procedure was devised to attain a tip speed ratio close to the design point claimed by the BEMT model. This is a key requirement to ensure the comparison of the power curves from the CFD, BEMT, and experimentation.

There were a total of 12 experiments performed at different loads and different wind speeds. At first, we placed the wind turbine 80 cm away from fans. A load of 1.5 Ω was connected to the turbine. All fans were turned on once and the turbine perform a steady-state test. When the turbine started rotating, we measured wind speed at the tip of the blades, and once again the average value of wind speed was calculated using an anemometer. Data was recorded for at least 4-5 minutes so that turbine should reach the constant angular velocity at 80 cm. in this case average value of wind speed was

4.6 ms^{-1}. In the second step same procedure was repeated but the distance was changed to 140 cm and 200 cm with a wind velocity of 4.1 ms^{-1} and 3.7 ms^{-1} respectively.

Furthermore, several experiments were performed by changing the load i.e. 5Ω, 14 Ω, and 28 Ω. Wind speed was changed by varying the distance of the turbine from the fan. All the experiments were performed in a steady-state condition. Results were recorded till the angular velocity of the turbine became constant. Figure 4.4 shows the schematic diagram of the experimental setup.

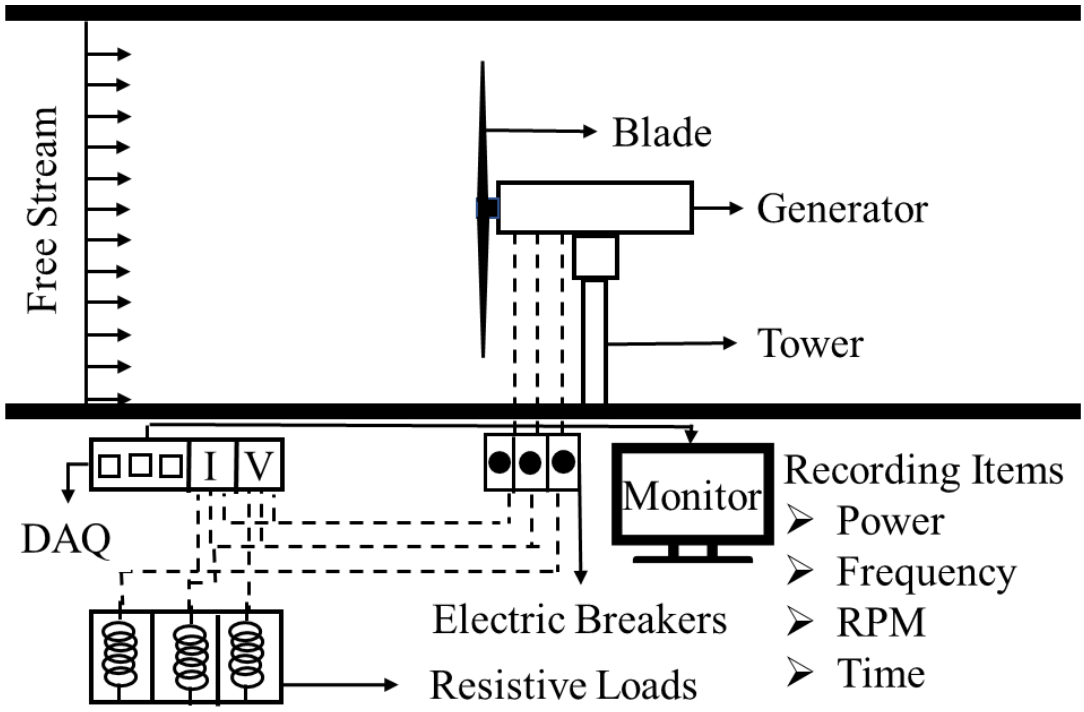

Figure 4.4 Schematic Diagram of the experimental setup

Wind tunnels are desirable to perform experiments on flow-related tests in a controlled environment. It was initially planned to conduct the test with a low-subsonic wind tunnel at the energy center but delays in setting up the wind tunnel forced us to opt for a manual arrangement. The testing conditions were controlled by arranging the setup in the wind tunnel shed. Further provisions were taken to ensure that no winds other than those created by the pedestal fans could enter the shed. The fans were kept well away from the walls on both sides and in front of the fans to avoid reflection of the flow streams. All the tests were conducted on sunny summer days and at the same time of a day, this was important to maintain the same thermal conditions that inside a warm shed could lead to temperature stratification and if the setup is placed close to a door

or a window, wind flows in and out of the room can cause significant variations. Moreover, the shed was prevented from any sort of indoor space cooling ahead of and during the experimentation

Table 4.2 List of experiments performed

Experiment No.	Load (Ω)	Distance (m)	Wind Speed(ms^{-1})
1	1.5	80	4.6
2	1.5	140	4.1
3	1.5	200	3.7
4	5	80	4.6
5	5	140	4.1
6	5	200	3.7
7	14	80	4.6
8	14	140	4.1
9	14	200	3.7
10	28	80	4.6
11	28	140	4.1
12	28	200	3.7

4.5 Calculations

4.5.1 Coefficient of Power (C_p)

The coefficient of power represents the efficiency of the wind turbine. C_p is the ratio of output power generated by the wind turbine and total available power from wind at a particular speed.

$$C_p = \frac{P}{\frac{1}{2}\rho A V^3 \eta} \tag{28}$$

Where P is the output power, ρ is air density i.e. 1.23 kg m^{-3}, V is the incoming wind velocity, η is the generator efficiency and A is the swept area of the wind turbine rotor which is given by πr^2.

$$C_p = \frac{P}{\frac{1}{2}\rho(\pi r^2) V^3 \eta} \tag{29}$$

$$C_p = \frac{15.257}{\frac{1}{2}(1.23)(3.14)(0.625)^2(4.6)^3(0.8)} \quad (30)$$

$$C_p = 0.28 \quad (31)$$

4.5.2 Rotation Per Minute (rpm)

RPM represents the number of cycles per minute of the rotor which is calculated by mechanical frequency recorded by DAQ.

$$N = \frac{2 \times 60 \times f}{P} \quad (32)$$

Where f is the mechanical frequency and P is the number of poles i.e., 10.

$$N = \frac{2 \times 60 \times 34.37}{10} \quad (33)$$

$$N = 401 \quad (34)$$

4.5.3 Tip Speed Ratio (λ)

TSR is the ratio between the tangential velocity of the rotor and the wind speed (V). TSR should be optimal if the TSR is too low turbine rotor will move very slow and ultimately stop, if its too high rotor will move swiftly through turbulent airflow that can cause mechanical failure of a wind turbine.

$$TSR(\lambda) = \frac{Tip\ Speed\ of\ Blade}{Wind\ Speed\ (V)} \quad (35)$$

$$TSR(\lambda) = \frac{R\omega}{V} \quad (36)$$

$$TSR(\lambda) = \frac{2\pi r(N)/60}{V} \quad (37)$$

$$TSR(\lambda) = \frac{2 \times 3.14 \times 0.625(401)/60}{4.6} \quad (38)$$

$$TSR(\lambda) = 5.71 \quad (39)$$

Summary:

This chapter includes all the experimentation done during this work. The chapter starts with the list of equipment required to perform experiments. After that chapter includes how the whole experimental setup was designed and how many experiments were done. The end chapter concludes with calculations of C_p, rpm, and tip speed ratio.

Chapter 5 Results and Discussion

5.1 Sensitivity of TSR to wind speed and load

The experimental setup for this study is a manual configuration of wind resources, electrical loads, and required sensors. Therefore, it is critical to calibrate the individual components of the experiment and design a combination that would provide us with the desirable experimental conditions. It has been identified earlier that the performance parameters of the new optimized turbine are available from BEMT modeling and CFD. Thus, a major aim of the experimental analysis is to achieve tip speed ratios as close to possible to those claimed by BEMT modeling and the CFD analysis. Hence, this experiment relies on two independent variables that influence the tip speed ratio of this small wind turbine. Wind speed is indeed the first variable that can be adjusted to achieve the desired tip speed ratio and there is a limit on the higher velocity that we can achieve with the four pedestal fans. Electrical loads being the second which can change vary the rotational speed of the turbine. Different loads were applied of which 1.5 ohms are the desired load which used be used to achieve the desired tip speed ratio but at the same time, there is a limitation of wind speed used by pedestal fans. In this situation, the position of the fans from the wind turbine is the only way besides the controllers on the fans to adjust the wind speed. Some experiments were performed to figure out the maximum velocity that could be attained with the fans. It was for 80 cm from the turbine to the fans where the maximum velocity of 5 m/s was observed but the average wind speed for repeated experiments for the same distance was 4.6 m/s. At such wind velocities, the maximum tip speed ratio is hardly in the range of 1 to 2. Therefore, another variable is required to combine with the available range of wind speed to reach a tip speed ratio close to 6, for which both BEMT and CFD provide power characteristics. The function of tip speed ratio is also driven by the angular velocity of the turbine, which in turn is dependent on the resistive torque that is induced by the electrical load connected to the turbine. It has been noticed by researchers that the electrical load does impact the starting time and performance of small wind turbines [1].

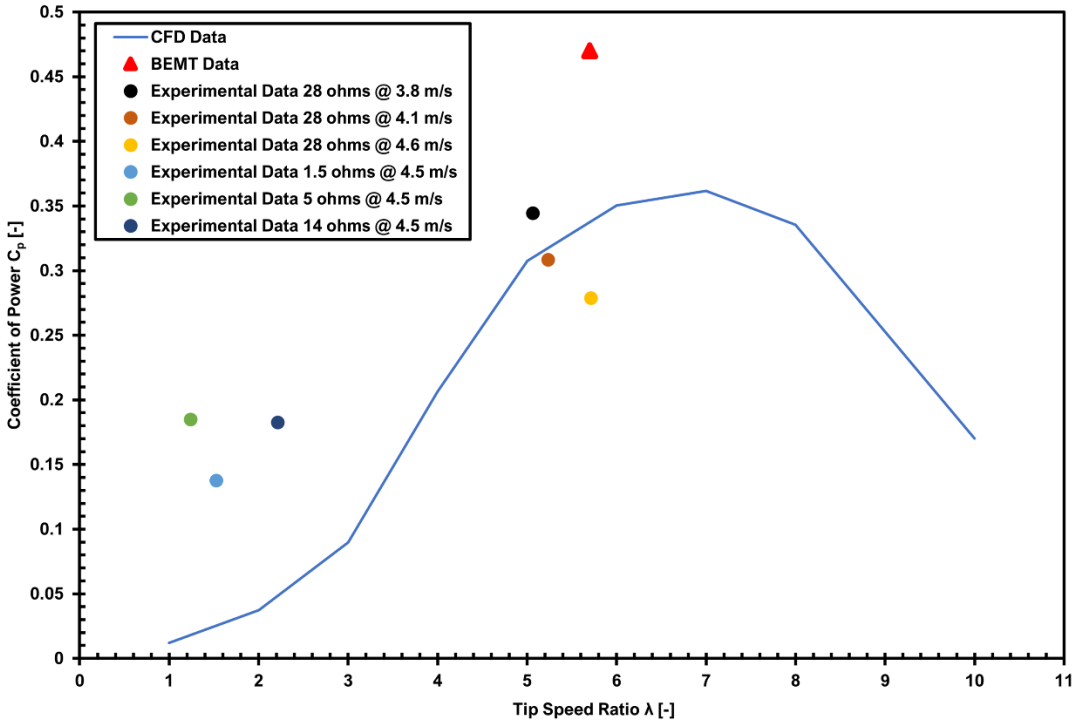

Figure 5.1 The coefficient of power against tip speed ratio for various wind speeds and electric loads

Based on these findings, various electrical loads were designed and tests to identify the influence on the tip speed ratio. As shown in figure 5.1, the tip speed ratio for the same wind speed but variable loads do vary and that indicates the influence of load on the rotational velocity of the turbine. More precisely, the points indicated for the loads less than 28 Ohms, the TSR is only 2.5, which is half less than what is required. A higher tip speed ratio for these could be achieved by increasing the incoming velocity, which could only be done by using a wind tunnel. By increasing the load to 28 Ohms the time speed ratio increases to 5 for a range of velocities from 3 m s-1 to 4.6 m s-1. Resistive loads for higher value i.e., greater than 28 ohms do have less electrical resistance and draw more current for which the turbine can easily overcome the starting torque. Figure 5.1 also indicates the variation of TSR for the same load and variable wind speed. For load 28 ohms at 4.1 ms-1 power coefficient is 0.31 much better but at a low tip speed ratio i.e., 5.2. The power coefficient for 28 ohms at 3.7 ms-1 is 0.35 best among all but the desired tip speed ratio of 5.02 is achieved which is not desirable. The combination of 28 Ohms and 4.6 m/s velocities provides a TSR of 5.71. Now that the experimental setup attains the necessary TSR, the remaining experiments were performed at 4.6 m/s wind speed and 28 Ohms electric load.

Table 5.1 TSR and C_p of simulated and experimental data

Sr. No	Results	Tips Speed Ratio (λ)	Coefficient of Power (C_p)
1	Experimental	1.52	0.13
2	Experimental	1.23	0.18
3	Experimental	2.2	0.18
4	Experimental	5.71	0.27
5	Experimental	5.23	0.30
6	Experimental	5.06	0.34
7	BEMT	5.7	0.47
8	CFD	5	0.30
9	CFD	6	0.35

In the perspective of power characteristics, these experiments reveal that the power outputs at lower TSR values are considerably higher than those predicted by CFD. However, at higher loads, i.e., 28 Ohms, the C_p is lesser than the corresponding value on the CFD curve and that is predicted by the BEMT model. This might have been caused because of the optimized design for a quicker starting time at the cost of some power loss. This is discussed in detail in a later section dedicated to performance analysis.

5.2 Time series of power and RPM

Small wind turbines are usually analyzed for starting time and cut-in velocities. This section of the paper presents the actual time series of the power outputs and angular velocities of the optimized wind turbine. In figure 5.2, the variation of power output in watts concerning time in seconds is plotted. It can be seen on that graph that the turbine starts to produce some power at 0.998 seconds, which is indeed the starting time of the turbine. The power output increases at a higher rate in the initial 10 seconds and afterward the increment in speed is rather slower until it becomes steady at 27 seconds to produce a maximum of 15 W power.

Figure 5.2 shows the variation of the rotational speed of the turbine with time. The behavior of rotational speed is like the power output curve. The first reading of RPM is recorded to be 50 for just 2 seconds since the flow is directed to the turbine. The slope of the increase in RPM is higher for the initial 10 seconds where the RPM reaches 250. The gradient of the curve appears to decrease as the RPM gradually increases to the maximum of 400 and becomes steady.

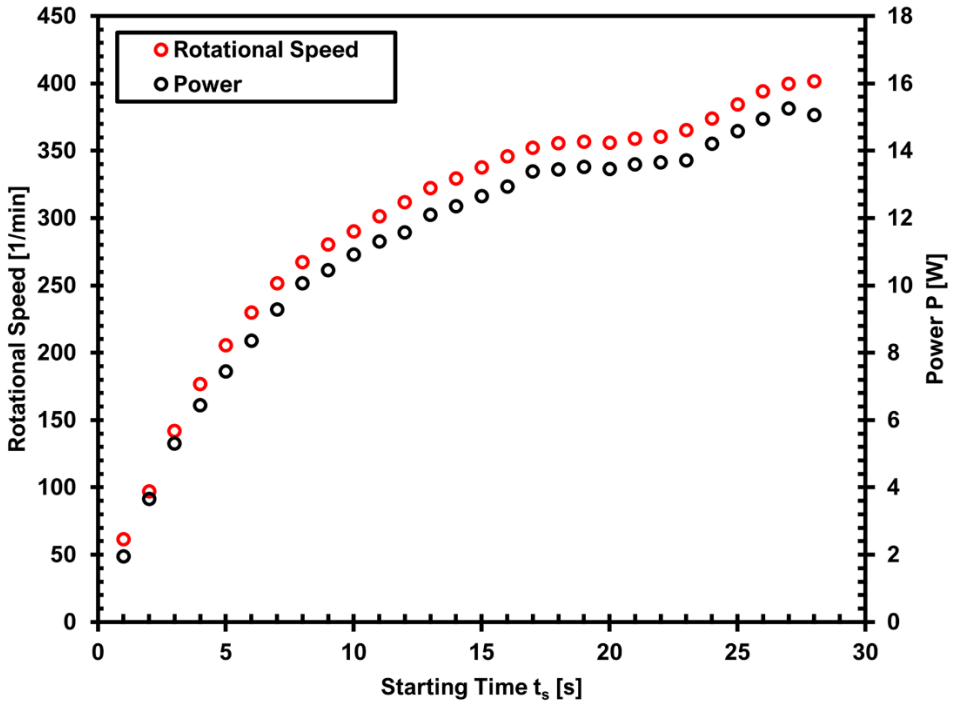

Figure 5.2 Time series of (a) power output and (b) rotational speed

5.3 Starting time and cut in speed

Starting time and cut in speed being the objective of the research. Hence it can be seen in the above figure starting time of the new optimized blade is approximately 1 second and a manual approach to finding the speed cut was used. The minimum velocity which could be achieved by the four pedestal fans we 3 m s^{-1}. So, 3 m s^{-1} was considered to be the cut-in speed of this optimized blade. At 3 m s^{-1} very less power output was achieved with less tip speed ratio. Normally the cut-in speed for a small wind turbine lies between 2-4 m s^{-1}.

5.4 Power profiles against angular velocity and wind speed

It is one of the major concerns of wind turbine designers to maximize the power output. The power output function depends on various external and internal parameters of the wind turbine. The mechanical and electrical components are internal parts of the turbine that impact the power outputs. Likewise, the kinetic energy in the wind stream is an external parameter that directly relates to the power output of a wind turbine. To inspect the power characteristic of the turbine design under consideration, the power for 28 ohms at different wind speeds is plotted against the rotational speed of the wind

turbine in figure 5.3 (a). This graph shows the power production capability of the wind turbine at various angular velocities. For RPM close to 50, the turbine can produce only 2 W of power. But the power output appears to increase linearly with increasing angular velocity. At the highest RPM of 400, the turbine produces 15 W power for wind speed at 4.6 m/s.

To analyze this aspect, the electric load was kept constant, and the velocity was varied. For 28 Ohms load, the turbine can produce up to 11.5 W power at the wind speed of 3.8 m/s. With the increase in velocity the power output increases to 13 W at 4.1 m/s and 15 W at 4.6 m/s. In general, the available power is directly proportional to the cube of the incoming velocity, therefore the curve for power variation with wind speed is not linear. It can also be inferred that the rated velocity of the wind turbine is way beyond 4.6 m/s and the complete power curve with velocity can only be achieved by performing experiments with wind velocities from cut-in to proposed cut-out velocities.

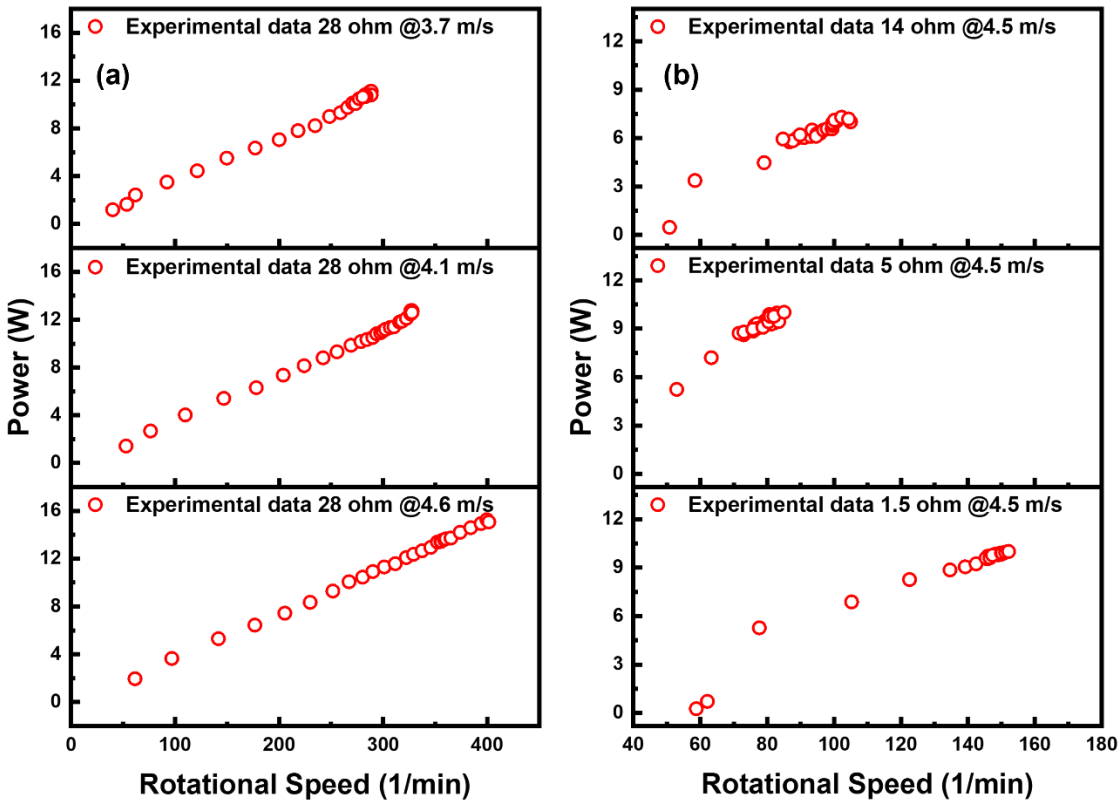

Figure 5.3 Power characteristics of the optimized rotor against (a) rotational speed at same load (b) different loads

In figure 5.3 (b) graph shows the power production capability of the wind turbine at various angular velocities for different resistive loads. For RPM close to 50, the turbine can produce only 2 W of power. For loads 14 ohms and less, maximum rotational speed 155 was achieved. But the power output appears to increase linearly with increasing angular velocity. At the highest RPM of 155, the turbine produces 10.5 W power for wind speed at 4.6 m/s.

5.5 Comparison of C_p for BEMT, CFD, and Experiments

The optimized novel design is now experimentally tested for power features. Previously, the blade design is inspected by both BEMT and CFD. In this part of the discussion, the values of the power coefficient claimed by each method used are compared to validate the previous studies. BEMT modeling can be both an analytical and a numerical process. Irrespective of that, the method heavily relies on the aerodynamic coefficients of the blade. In that way, BEMT modeling is prone to uncertainties in its results as the airfoil data is either provided by wind tunnel testing or airfoil design software. The Cp curve predicted by CFD, and the two points provided by BEMT, and experiments are shown in figure 5.4 below. The data reveals that the BEMT model had overestimated the Cp by about 40.60 % than that of the experimental values at 5.7 TSR. The CFD results were still closed but that too overestimated the power output by 17.95 %. However, a power coefficient of 0.27 against TSR of 5.71 is still appreciable to approve the design for urban utility. Moreover, the highest Cp for the design might occur at higher TSR that this experimentation did not execute yet. There could also be slight experimental errors for the manual approach used to perform the experiments. Therefore, it is strongly recommended to perform wind tunnel testing of the design to reveal all the features of this new blade design.

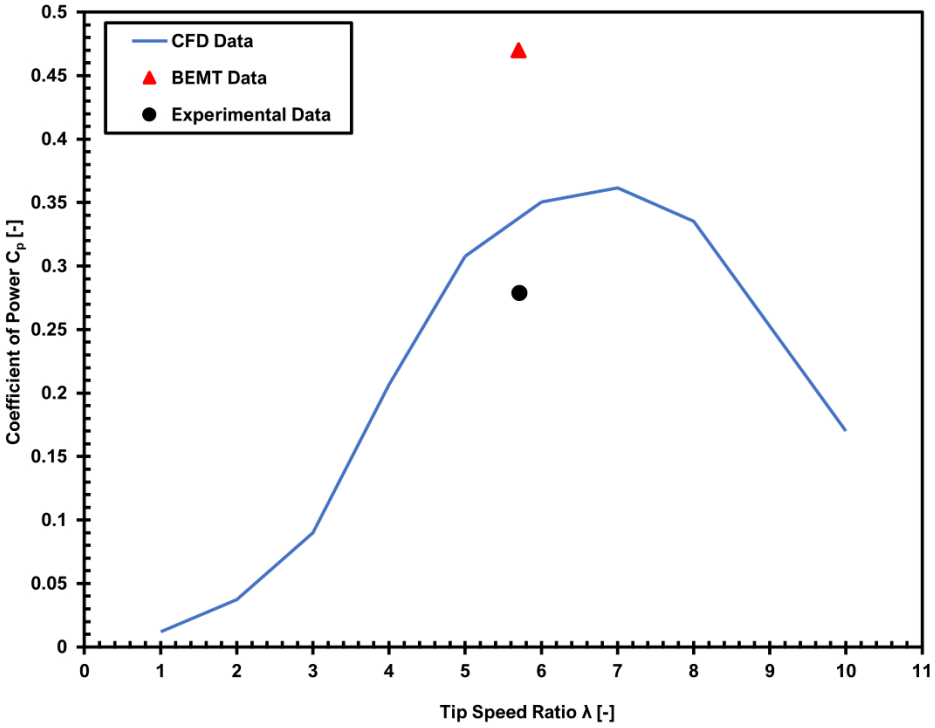

Figure 5.4 The comparison of power coefficient for CFD, BEMT, and experiment.

Summary:

Chapter five discusses results concluded from experimentation. It discusses the sensitivity of TSR to wind speed and load and time series of power and rpm. Cut in speed and starting time of turbine are discussed. In the end, a comparison of our experimental results was compared with the results of BEMT and CFD.

Chapter 6 Conclusion and Recommendations

6.1 Conclusion

This experimental study successfully executes the testing of a novel optimized micro-scale wind turbine in a controlled environment by designing a setup that is a configuration of available testing components. This research also provides the real data to compliment the previously performed modeling of the same turbine design. The main conclusions of the research are enlisted below.

- The experimental setup aimed to achieve tip speed ratios close to 6, to acquire performance characteristics of the turbine that can be compared with the performance claimed by the Blade Element Moment Theory and Computational Fluid Dynamics modeling methods. It was found that the tip speed ratio is influenced by both wind speed and the electric load. Thus, both parameters are combined to achieve the desired tip speed ratio.
- The inertial mass of the 3D printed blade was a major concern hence Polylactic Acid (PLA) was used. Mass of procure blade of WUXI turbine was 214 g. PLA has a density of 1.25 g cm^{-3} was selected for 3D printing. New 3D printed blade had a mass of 213.4 g.
- The blade design is deemed optimized for quick starting time and still, optimal power outputs considering the weight factor 0.7 i.e., 30 % coefficient of performance and 70% starting time. The time series of power output and the angular velocity of the turbine reveals that the turbine shall start within 0.998 seconds of the flow incidence onto the rotor whereas starting times claimed by BEMT and 6DOF are 2.8 s and 3.25 s respectively.
- The experimental cut-in speed for the optimized blade is 3ms-1 being much better than numerical analysis i.e., 5 m s^{-1}.
- The power characteristics of the turbine claimed by the modeling methods appear to be overestimated. The experimental value of the coefficient of power lags both BEMT and CFD by 40.60 % and 17.95 %, respectively.

- Power outputs shown by the experimentation are higher at tip-speed ratios close to 5 but for higher tip speeds the power outputs are lower.

6.2 Recommendations

Although this research presents the promising potential of reduced cut-in speed and improved starting time of the prototyped 3D printed polylactic acid blades there are some essential aspects of rotor design such as structural analysis of rotor to give a holistic view and proposal for baseline and improved design, there are some recommendations for future work on this topic enlisted below:

- To conduct the finite element analysis of both designs to assess which design is structurally safe and robust, and which is more susceptible to failure.
- Instead of prototyping a scaled-down 3D printed blade for 200W, research should be done on prototyping experimentation of a 1 KW wind turbine.
- In the future, experimentation should be performed using oak wood and instead of polylactic acid as a blade material.
- New experiments should be performed using industrial fans or wind tunnel diffusers as their wind speed can be controlled.
- Future experiments should be conducted in outdoor conditions to get more accurate and realistic results.

Acknowledgments

First and foremost, I am thankful to Almighty ALLAH who is the creator and author of knowledge. Indeed, without YOUR blessings, this mammoth task would not have been possible. And I acknowledge that without YOUR willingness and guidance, I would not have done a single task.

I am grateful to my parents for their unconditional love and sacrifices. I am forever in your debt for your encouragement, financial and moral support. Thank you for keeping confidence in me.

I express my sincerest gratitude to **Dr. Adeel Javed** for this opportunity, for your teaching, mentorship, and patience throughout the research. It has been truly a privilege to work with you. I would like to thank my GEC members **Dr. Sehar Shakir, Dr. Majid Ali** and **Dr. Hassan Abdullah Khalid** for their guidance and help throughout my research.

I am also thankful to the staff of Thermal Energy Lab specially Engineer **Hassan Nazir,** Biofuel lab Engineer **Mr. Ali Abdullah,** Smart Grid lab engineer **Mr. Saeed Iqbal** and Mechanical Workshop Technologist **Mr. Qamar Ud Din** who helped in my research and gave valuable advice during my experimentation. I am also grateful to the other lab staff, faculty members, and administration who were a part of this journey. I profusely thank my father **Kanwar Muhammad Abid** for his immense support, always being there for me whenever I needed help. Also, all my friends for their support both academically and in general. And to life, an extraordinary experience with so many things to enjoy within a short span. Thank you for giving me so much in the years past, and for more to discover in the years to come.

Appendix 1 - Publication

“Experimental Investigation of an Urban-Scale Horizontal Axis Wind Turbine Rotor Optimized for Improved Starting Performance in Low Wind Speed Conditions”

Ahmad Zubair Hashim, Adeel Javed, Saeed Iqbal, Syed Ali Abbas Kazmi

Abstract

Optimizing a blade for a small wind turbine to achieve a quick starting time at the loss of minimal power output is one of the most challenging aspects of design. This study considers a micro-wind turbine for experimental analysis to validate an optimized blade design based on blade element momentum theory and its performance analysis conducted numerically. A scaled-down rotor of three blades optimized for both quick starting time and optimum power was manufactured by 3D printing. The blades were mounted on a hub of a commercially available Wuxi 200W wind turbine to carry out the experimental analysis in a controlled environment. Both wind speed and electric resistive loads were varied to achieve the desired tip speed ratio. It was observed that the rotational speed of the micro-wind turbine is affected by the resistive torque induced by the electric loads connected to the circuitry of the permanent electric generator. After the experiments, it was inferred that the optimized blade is well justified to operate in low wind conditions. The power outputs claimed by both blade element momentum theory and computational fluid dynamic analysis of the blade lag 40% and 17%, respectively. However, the experimental investigation shows superior starting time performance as it leads both the BEMT model and 6DOF analysis by 2.8 s and 3.25 s, respectively. The observed power coefficient at the tip speed ratio of 5.71 is 0.28 and that of the staring time is just 1 s. Therefore, this optimized blade design for micro-wind turbines is desirable for urban environments with wild wind resources.